https://doi.org/10.5194/egusphere-2024-3057
Preprint. Discussion started: 23 October 2024

Strong inter-model differences and biases in CMIP6 simulations of $PM_{2.5}$, aerosol optical depth, and precipitation over Africa

Catherine A. Toolan[1], Joe Adabouk Amooli[2], Laura J. Wilcox[3], Bjørn H. Samset[4], Andrew G. Turner[1,3], and Daniel M. Westervelt[2,5]

[1]Department of Meteorology, University of Reading, Reading, United Kingdom
[2]Lamont-Doherty Earth Observatory of Columbia University, Palisades, NY, United States of America
[3]National Centre for Atmospheric Science, University of Reading, Reading, United Kingdom
[4]Center for International Climate and Environmental Research (CICERO), Oslo, Norway
[5]NASA Goddard Institute for Space Studies, New York, NY, United States of America

Correspondence: Catherine A. Toolan (c.toolan@pgr.reading.ac.uk)

Abstract. Poor air quality and precipitation change are strong, rapidly changing, and possibly linked, drivers of physical hazards in sub-Saharan Africa. Future projections of sub-Saharan air quality and precipitation remain uncertain due to differences in model representations of aerosol, aerosol-precipitation interactions, and unclear future aerosol emission pathways. In this study, we evaluate the performance of CMIP6 models in simulating $PM_{2.5}$, aerosol optical depth (AOD), and precipitation over Africa, relative to a range of observational and reanalysis products, including novel observational datasets, over the 1981-2023 period. While models accurately capture the seasonal cycle of PM2.5 concentrations over most regions, the concentration magnitudes show strong inter-model diversity. Dust AOD shows generally accurate seasonal spatial distribution, with multi-model mean (MMM) pattern correlation coefficients within 0.77-0.94, despite strong inter-model diversity in magnitude. Seasonal spatial patterns of non-dust AOD are poorly represented, with MMM pattern correlation coefficients of 0.25-0.58, and poorest performance during SON. Emission inventory inaccuracies may explain systematic biases for non-dust AOD fields, with differences in circulation and precipitation patterns, and aerosol treatment causing inter-model diversity. Both monsoon regions are generally well captured, though there is poorer performance in simulating the east African monsoon. Biases found relate to the intertropical convergence zone, more apparent over east Africa, and rainfall magnitude, more apparent over west Africa. This evaluation highlights strong inter-model diversity in the representation of African air quality and climate, and identifies model performance over sub-Saharan Africa, and the reasons behind the biases, as critical gaps to address for improving confidence in climate projections.

1 Introduction

Africa is a region of large heterogeneity in both air quality and precipitation (Hulme, 2001; Bauer et al., 2019). Variations in air quality are not well characterized due to a scarcity of long-term observations (United Nations Environment Programme, 2017). However, initial studies of individual regions in Africa (Kalisa et al., 2023; Kebede et al., 2021) have shown high spatial

https://doi.org/10.5194/egusphere-2024-3057
Preprint. Discussion started: 23 October 2024

and temporal variability on interannual and multidecadal timescales. Precipitation variability is manifested in severe drought conditions and floods, often affecting the same region from year to year (Lüdecke et al., 2021).

The variability of air quality and precipitation both have strong impacts on public health. For example, air pollution was the second highest risk factor for mortality across Africa in 2019 (Health Effects Institute, 2022; Xing et al., 2016), placed above that associated with unsafe water, sanitation, and hygiene. Africa exhibits high levels of $PM_{2.5}$ (McFarlane et al., 2021; Raheja et al., 2023; Westervelt et al., 2023) — aerosols with an aerodynamic diameter of less than 2.5 μm (Seinfeld and Pandis, 2016). High concentrations of $PM_{2.5}$ are a known cause of increased morbidity and mortality (Xing et al., 2016), so capturing the evolution of $PM_{2.5}$ is essential for mitigation strategies. The second leading cause of illness burden in most of sub-Saharan Africa is household air pollution from solid fuels, which adds to ambient particulate matter pollution (Katoto et al., 2019). Air quality is undergoing changes, with a continent-wide increase in aerosol emissions associated with population growth, urbanization, and industrialisation (Wei et al., 2021), demonstrated by increasing AOD and higher $PM_{2.5}$ levels over the majority of Africa (Turnock et al., 2020). Africa has undergone, and continues to undergo, strong variations in annual precipitation. Drought in the Sahel from 1968 to 1973 was marked by a sudden shift from the wetter regime of the 1960s to a multi-year dry anomaly (Hulme, 2001). The drought was found to be directly linked to an estimated 100,000 deaths (Copans, 2019), as well as leading to the loss of 40-60% of livestock in the region (Glantz, 1976). While annual mean precipitation has steadily recovered since 1983 in the western Sahel (Porkka et al., 2021), the eastern coast of Africa has experienced further drought conditions, with the Greater Horn of Africa undergoing its most severe drought in 40 years between 2018 and 2023 (World Health Organisation, 2024).

$PM_{2.5}$ concentrations relate to the large-scale behaviour of AOD and precipitation patterns, as well as local aerosol emissions. $PM_{2.5}$, AOD, and precipitation all exhibit interlinkages at different spatial scales. AOD and $PM_{2.5}$ concentration are closely linked, as both are measures of particulate matter in the atmosphere. However, the variables do not necessarily align spatially with each other, due to differences in sources and compositional differences, and the fact that $PM_{2.5}$ is generally measured at the surface while AOD is a whole-column measurement that also takes aerosol radiative properties into account. Aerosol concentration changes induce radiative forcing directly through the extinction of incoming solar radiation and indirectly through the modification of cloud microphysical properties (Boucher et al., 2013; Samset et al., 2018; Westervelt et al., 2020). Enhanced aerosol levels increase cloud condensation nuclei (CCN) concentrations (Twomey et al., 1984) resulting in more numerous but smaller cloud droplets, which increases cloud albedo and potentially increases cloud lifetime (Twomey, 1977), and can affect the efficiency of precipitation formation and the size distribution of raindrops (Westervelt et al., 2017; Gupta et al., 2023; Stier et al., 2024; Levin and Cotton, 2008). In addition, temperature profile modifications through heating due to absorbing aerosols alter atmospheric stability, changing cloud cover and therefore impacting the Earth's albedo (Ramanathan and Carmichael, 2008). Absorbing aerosols also strongly affect precipitation, through changes to the local energy balance and lapse rates (Williams et al., 2023; Samset, 2022). The strongly regional radiative forcing due to aerosol changes also leads to changes in the atmospheric circulation, both local to and remote from the aerosol changes. It has been shown in previous studies that African precipitation is affected by aerosol emissions, from both local and remote sources (Monerie et al., 2023; Scannell et al., 2019; Shindell et al., 2023).

https://doi.org/10.5194/egusphere-2024-3057
Preprint. Discussion started: 23 October 2024

Conversely, precipitation also impacts air pollution, causing removal of aerosols from the atmosphere via wet deposition (Fuzzi et al., 2015; Wang et al., 2023) and influencing dust emissions via soil moisture, so changes in precipitation can cause feedbacks. Thus, it can be expected that relationships exist between African air quality and precipitation, though the response of precipitation to changes in aerosol emissions is dependent on the background state of both the emission and response region (Persad, 2023).

The African continent is associated with both high biomass burning in tropical forests and intense dust storms from the Sahara Desert. Both are strong sources of atmospheric pollutants, for gaseous and aerosol species (Booyens et al., 2019). Performance in simulating airbourne particulate matter is very diverse across Coupled Model Intercomparison Project Phase 6 (CMIP6) models, as varying representations and parameterizations of differing numbers of aerosol species result in strong differences in AOD between models (Fiedler et al., 2023). For example, Zhao et al. (2022) found that global dust emissions varied by a factor of 5 across 16 CMIP6 models, and noted large uncertainties in the simulated dust processes. In addition, there is some disagreement in observations and reanalysis datasets for AOD over Africa; there is a factor of 2 difference in dust burden between the CAMS and MERRA2 reanalyses (Zhao et al., 2022). This is an important source of intermodel disagreement over Africa, as dust contributes strongly to AOD over northern areas of the continent, as seen in Figure 1. In addition, nitrate aerosol, one of the major contributors to $PM_{2.5}$, as well as AOD, is not modelled by most CMIP6 models (Archer-Nicholls et al., 2023), contributing to strong intermodel spread, and worsened performance compared to observations. Evaluation of $PM_{2.5}$ levels for CMIP6 over Africa has not yet been performed due to a lack of appropriate observational data, and this analysis presents an opportunity to better understand the projections of health risk from $PM_{2.5}$; if the CMIP6 models are producing incorrect $PM_{2.5}$ concentrations, then this could lead to overestimating or underestimating how often dangerous levels of $PM_{2.5}$ are reached, with knock-on effects on estimates of mortality.

CMIP6 models (Eyring et al., 2016) are known to have biases relative to observations in both African rainfall and air quality (Woodward et al., 2022). Precipitation biases occur spatially, for example in the southward bias of the tropical rainband, which has persisted for several generations of CMIP (Bock et al., 2020), and temporally, for example the progression of the monsoons over east and west Africa (Annor et al., 2023; Ayugi et al., 2021). The spatial biases are mostly found over west Africa, whereas biases in the timing of the seasonal cycle are found over both east and west Africa. Finding the root cause of these precipitation biases has proven difficult; previous work has suggested that sea-surface temperature (SST) biases could be to blame (Schwarzwald et al., 2023). Other proposed causes include difficulties simulating the Saharan heat low (SHL) (Dixon et al., 2017), as well as the meridional soil moisture gradient between the Sahara and Gulf of Guinea discussed in Cook (1999). These previous studies focused on either east or west Africa, while this study applies consistent evaluation approaches across the continent, with a focus on both regions.

As there are longstanding biases in precipitation over Africa in CMIP6 which are not explained by coupled SST biases (Schwarzwald et al., 2022), there may also be interlinkages between the performances of precipitation and air quality over Africa, given established interactions between the two. The reasons behind the biases in air quality and precipitation over Africa are not well understood, and this is a clear area for improvement in CMIP6 models. These biases mean that future projections, which also contain high uncertainty for African aerosol emissions under different socioeconomic pathways, are

https://doi.org/10.5194/egusphere-2024-3057
Preprint. Discussion started: 23 October 2024

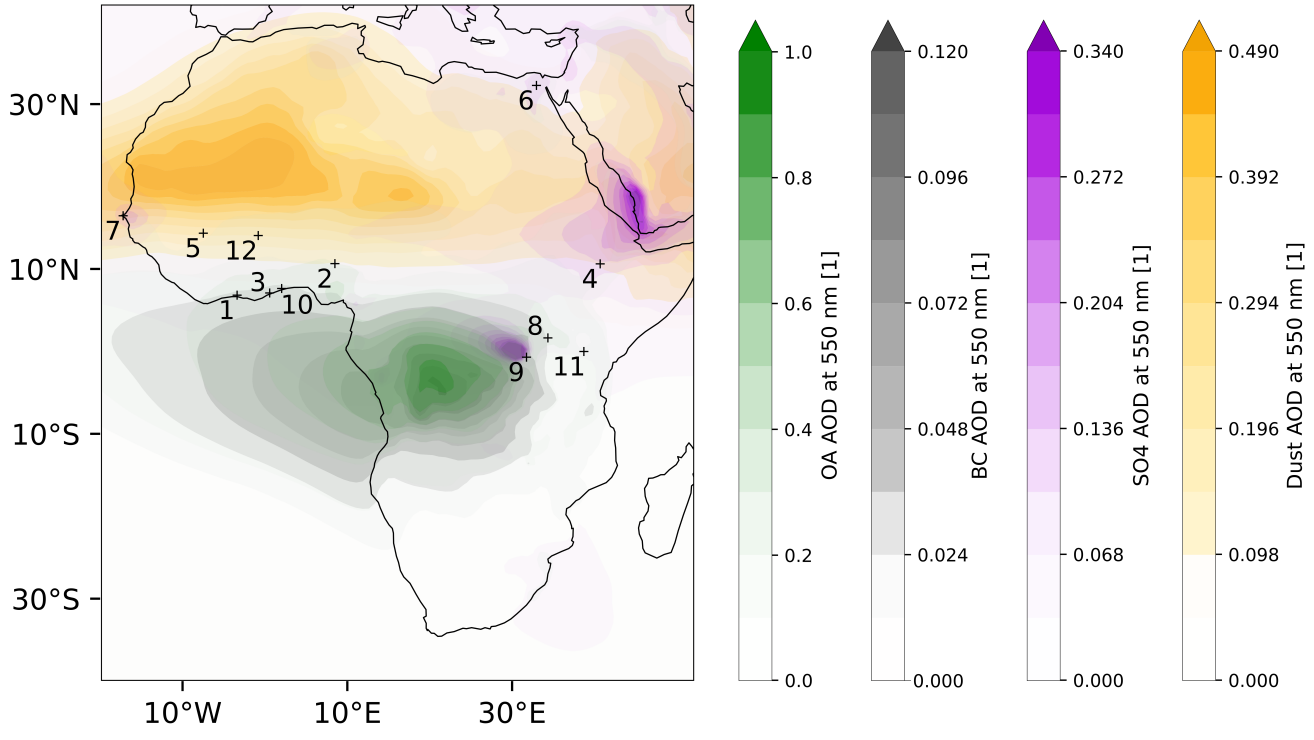

Figure 1. AOD contributions from organic aerosol (OA) (green), black carbon (BC) (black), sulphate (SO_4) (purple), and dust (yellow) over Africa for SON in the CAMS reanalysis over 1981-2023. Numbered points indicate the location of the $PM_{2.5}$ observation stations used in this analysis (see Table 1 for details of locations). AOD is unitless.

very poorly constrained (Wells et al., 2023). In addition, as the mechanisms through which the two affect each other are not well quantified (Myhre et al., 2013), the uncertainty in the future evolution of air quality and precipitation is compounded. There is a need for models which can capture air quality and precipitation over Africa accurately to inform policy-making and adaptation strategies in the face of climate change. Due to the risks to human health from changes in air pollution and precipitation, as well as their potential feedback interactions, both factors are discussed jointly in this study.

In this study, our aim is to identify areas of strong and weak performance in CMIP6 models over Africa, so that understanding of the biases and overall performance can be used to understand how CMIP6 models respond to future emissions pathways. We demonstrate the performance of CMIP6 models in replicating $PM_{2.5}$ concentrations in 12 cities around Africa, through timeseries demonstrating both the annual cycle and interannual variability. Expanding into the representation of larger scale features, we evaluate the performance of CMIP6 models for AOD, examining the seasonal spatial distribution of AOD over the whole of Africa, as well as the performance of regional annual cycles in AOD and their interannual variability. Explor-

https://doi.org/10.5194/egusphere-2024-3057
Preprint. Discussion started: 23 October 2024

ing the performance of CMIP6 models in Africa further, model evaluation is performed for CMIP6 models' seasonal spatial distribution of rainfall over the whole of Africa, and representation of the regional African monsoon systems. Changes in $PM_{2.5}$ concentrations are only available from 2016 onwards, due to observational data scarcity over Africa (Shindell et al., 2022). This study evaluates all CMIP6 models for which the necessary simulations were available, while also highlighting models participating in the Regional Aerosol Model Intercomparison Project (RAMIP) (Wilcox et al., 2023). RAMIP consists of experiments designed to quantify the role of global and regional aerosol emissions changes in near-term projections, including experiments that focus on African emission changes. Given that aerosols have strong impacts on African precipitation, evaluating the performance of these models over Africa will be instrumental in interpreting the results of RAMIP.

In Sect. 2.1 we introduce the observational and reanalysis datasets used for this study, including the introduction of a new $PM_{2.5}$ observation dataset for Africa. These observations are comprised of in situ measurements of $PM_{2.5}$ for several regions in east and west Africa, and, while each location has a different start date for its time series, the earliest measurements are from 2016. This dataset has not yet been compared to CMIP6 model output, and so this study is the first to take the opportunity for observation-based evaluation of CMIP6 performance for $PM_{2.5}$ over Africa. In Sect. 2.2, we introduce the models evaluated. For Sect. 2.3, we discuss the evaluation metrics used. Sect. 3 shows the performance of the ensembles of models used, arranged by variable. In Sect. 3.2, we evaluate the performance of CMIP6 models against surface observations of $PM_{2.5}$ at different U.S. Embassy locations in Africa to ascertain model biases and inter-model differences. In Sect. 3.3, the AOD performance of CMIP6 models against reanalysis is evaluated, and in Sect. 3.4 the performance of precipitation in CMIP6 models against observations is evaluated. Sect. 4 summarises these results and discusses how they relate to future work on climate responses over Africa.

2 Methods

The analysis consists of an evaluation of the present day period in CMIP6, comprising 1981-2023, from a combination of the *historical* and *SSP3-7.0* experiments over Africa, against various observation and reanalysis datasets. The evaluation data are explained in Sect. 2.1, the models are listed in Sect. 2.2, while methods used are described in Sect. 2.3.

2.1 Observational and Reanalysis Datasets

The datasets used for the evaluation performed in this study are discussed in the following subsections. They include a range of in situ and remote-sensing observations, and meteorological and composition reanalyses.

2.1.1 Station $PM_{2.5}$ measurements

Data from surface air quality monitors at U.S. Embassy locations in Africa (noted in Table 1) were used for $PM_{2.5}$ evaluation, and obtained from the AirNow database (AirNow, 2021). These measurements began in 2016 at the earliest, although some stations only record data from 2023 onwards. The are 7 stations in west Africa and 4 in east Africa, shown in Figure 1. The datasets for east Africa are longer, extending back to 2016 and 2017 for Addis Ababa and Kampala. At each air quality

https://doi.org/10.5194/egusphere-2024-3057
Preprint. Discussion started: 23 October 2024

City	Country	Latitude (°N)	Longitude (°E)	Number
Abidjan	Côte d'Ivoire	5.334	-3.976	1
Abuja	Nigeria	9.041	7.477	2
Accra	Ghana	5.580	-0.171	3
Addis Ababa	Ethiopia	9.059	38.764	4
Bamako	Mali	12.630	-8.019	5
Cairo	Egypt	30.041	31.234	6
Dakar	Senegal	14.745	-17.526	7
Kampala	Uganda	0.300	32.592	8
Kigali	Rwanda	-1.936	30.078	9
Lagos	Nigeria	6.441	3.407	10
Nairobi	Kenya	-1.234	36.811	11
Ouagadougou	Burkina Faso	12.305	-1.497	12

Table 1. The positions of U.S. Embassies with AirNow $PM_{2.5}$ monitors that are used in this analysis. Number in the final column relate to points shown in Figure 1 and panel numbers in Figure 3

monitoring site, Met One Beta Attenuation Monitor 1020 (BAM-1020) sensors are installed, and are operated by the U.S. State Department. The BAM-1020 is a certified U.S. EPA Federal Equivalent Method monitor for ambient $PM_{2.5}$ concentrations (U. S. Environmental Protection Agency, 2011), which outputs real-time (hourly or finer) measurements of $PM_{2.5}$. The sensor uses beta ray attenuation by a filter-tape medium laden with size selected particles sampled from ambient air to calculate $PM_{2.5}$ concentration (Hagler et al., 2022).

2.1.2 Reanalysis AOD data

The Copernicus Atmospheric Monitoring Service (CAMS) reanalysis product is used for AOD evaluation (Inness et al., 2019). This dataset was used as it offers gridded data, facilitating the evaluation of AOD in regions of Africa with sparse observations from in situ monitoring stations such as AERONET (AERONET, 2024). It assimilates data from multiple satellite retrievals, so AOD in the reanalysis is well constrained by observations. The use of the reanalysis dataset also avoids issues that satellite-based observation datasets such as MODIS face, where surface brightness over deserts causes a lack of contrast between aerosol signal and the underlying surface brightness (Wagner et al., 2010), or where systematic biases are present when clouds interfere with optical measurements (Lee et al., 2013). While the dust optical depth over northern Africa is known to be too low, the CAMS reanalysis has been shown to perform well for mean AOD over this region, as well as capturing climatology and variability (Kapsomenakis et al., 2021). In this study, we evaluate both the AOD due to dust at 550 nm (dust AOD), and the AOD due to aerosols excluding dust at 550 nm (non-dust AOD = total AOD − dust AOD), to identify differences in performance between the dust and non-dust AODs. We evaluate AOD instead of aerosol burden, as dust AOD and non-dust AODs are widely available for the majority of CMIP6 models, and are directly comparable to the AOD reanalysis whereas aerosol

https://doi.org/10.5194/egusphere-2024-3057
Preprint. Discussion started: 23 October 2024

burden observations are scarce (Fosu-Amankwah et al., 2021). In addition, the AOD in CAMS is more tightly constrained than aerosol burden, through the assimilation of satellite observations (Garrigues et al., 2022), though the speciated AODs are more dependent on the underlying model (Inness et al., 2019).

2.1.3 Precipitation observations

The Climate Hazards Group InfraRed Precipitation with Station data (CHIRPS) (Funk et al., 2015) dataset, a land-only gauge-based rainfall dataset produced from blended station data from 1981 to near present, CRU (Mitchell and Jones, 2005), ERA5 (Hersbach et al., 2020), and GPCP (Huffman et al., 2023) were considered when choosing a reference observational or reanalysis dataset for this analysis. The CHIRPS product was chosen as it was specifically designed to monitor rainfall in the tropics, and it has been shown that CHIRPS has good performance relative to other datasets used to evaluate and monitor Africa and the tropics (Ayehu et al., 2018). Beck et al. (2017) found that CHIRPS ranked among the best performers in capturing precipitation indices and long-term precipitation means, but also noted that it underestimated peak magnitude of rainfall and produced spurious drizzle — which was found to be a common bias among the reanalyses evaluated. CHIRPS is intended for environmental monitoring so its performance in capturing low-frequency climate variability is not well-known. However, trends are seen to be well-represented over east Africa (Peterson et al., 2014), and while CHIRPS overestimates the frequency of rainfall, the rainfall contributed by these extra events is small (Diem et al., 2019).

2.2 Model datasets

In this study, we make use of all CMIP6 models for which the relevant outputs are available for the *historical* and *SSP3-7.0* simulation, to cover the 1981-2023 period. This means that there are more models evaluated for precipitation than AOD, and more evaluated for AOD than for $PM_{2.5}$ concentrations. However, understanding the range of model performance across the CMIP6 ensemble, without restricting the study only to models with all aerosol variables available, was a priority for the choice of models. We use the *historical* experiment from CMIP6, which includes time varying emissions of greenhouse gases, aerosols, and ozone, along with volcanic and solar forcing for the period 1981-2014, and the 'regional rivalry' shared socioeconomic pathway, *SSP3-7.0*, experiment from ScenarioMIP (O'Neill et al., 2016) for the period 2015-2023. The choice of a single scenario, *SSP3-7.0*, does not bias results here, since aerosol emissions do not diverge in the period used (Gidden et al., 2018). These datasets are concatenated before analysis.

The list of models used is shown in Table 2, with the nominal atmosphere and ocean resolutions also shown. Numbers assigned to each model are used to label them in later figures. In addition to the general evaluation of CMIP6 models, we highlight the performance of models participating in the Regional Aerosol Model Intercomparison Project (RAMIP). RAMIP includes experiments to explore the climate and air quality responses to near-future changes in African emissions of sulphur dioxide, black carbon, and organic carbon. As African climate has already been shown to be sensitive to remote aerosol changes (Scannell et al., 2019; Dong et al., 2014), it is anticipated that the African response to both local and remote changes in aerosol emissions will be a key focus of the analysis of RAMIP experiments. Evaluating the performance of participating models in replicating regional climate and air quality over Africa is therefore important before further work.

https://doi.org/10.5194/egusphere-2024-3057
Preprint. Discussion started: 23 October 2024

Centre	Model	Number	Data reference	Model reference	Number of ensemble members	Nominal Atmospheric Resolution	Nominal Ocean Resolution
CSIRO-ARCCSS	ACCESS-CM2	1	Dix et al. (2019)	Dix et al. (2019)	10	250 km	100 km
CSIRO	ACCESS-ESM1-5	2	Ziehn et al. (2019)	Ziehn et al. (2020)	40	250 km	100 km
AWI-CM	AWI-CM-1-1-MR	3	Semmler et al. (2018)	Semmler et al. (2020)	5	100 km	25 km
AWI	AWI-ESM-1-1-LR	4	Danek et al. (2020)	Sidorenko et al. (2015)	1	250 km	50 km
BCC	BCC-CSM2-MR	5	Wu et al. (2018)	Wu et al. (2019)	3	100 km	50 km
BCC	BCC-ESM1	6	Zhang et al. (2018)	Wu et al. (2020)	3	250 km	50 km
CAMS	CAMS-CSM1-0	7	Rong (2019)	Hao-Ming CHEN (2019)	3	100 km	100 km
CCCma	CanESM5	8	Swart et al. (2019a)	Swart et al. (2019d)	40	500 km	100 km
CCCma	***CanESM5-1***	9	Swart et al. (2019c)	Swart et al. (2019c)	20	500 km	100 km
CCCma	CanESM5-CanOE	10	Swart et al. (2019b)	Christian et al. (2022)	3	500 km	100 km
CAS	CAS-ESM2-0	11	Zhang et al. (2020)	Zhang et al. (2020)	3	100 km	100 km
NCAR	CESM2-FV2	12	Danabasoglu (2019a)	Danabasoglu et al. (2020)	3	100 km	100 km
NCAR	***CESM2***	13	Danabasoglu (2019c)	Danabasoglu et al. (2020)	11	250 km	100 km
NCAR	CESM2-WACCM	14	Danabasoglu (2019b)	Danabasoglu et al. (2020)	3	100 km	100 km
THU	CIESM	15	Huang (2019)	Lin et al. (2020)	3	100 km	50 km
CMCC	CMCC-CM2-HR4	16	Scoccimarro et al. (2020)	Cherchi et al. (2019)	1	100 km	25 km
CMCC	CMCC-CM2-SR5	17	Lovato and Peano (2020)	Cherchi et al. (2019)	1	100 km	100 km
CMCC	CMCC-ESM2	18	Peano et al. (2020)	Peano et al. (2020)	1	100 km	100 km
CNRM-CERFACS	CNRM-CM6-1	19	Voldoire (2018)	Voldoire et al. (2019)	30	250 km	100 km
CNRM-CERFACS	CNRM-CM6-1-HR	20	Voldoire (2019)	Voldoire et al. (2019)	1	100 km	25 km
CNRM-CERFACS	***CNRM-ESM2-1***	21	Seferian (2018)	Séférian et al. (2019)	8	250 km	100 km

https://doi.org/10.5194/egusphere-2024-3057
Preprint. Discussion started: 23 October 2024

E3SM-Project	E3SM-1-0	22	Bader et al. (2019a)	Golaz et al. (2019)	1	100 km	50 km
E3SM-Project	E3SM-1-1	23	Bader et al. (2019b)	Burrows et al. (2020)	1	100 km	50 km
E3SM-Project	E3SM-1-1-ECA	24	Bader et al. (2020)	Burrows et al. (2020)	1	100 km	50 km
E3SM-Project	E3SM-2-0	25	Bader et al. (2023)	Golaz et al. (2022)	1	100 km	50 km
CAS	FGOALS-f3-L	26	YU (2019)	He et al. (2020)	3	100 km	100 km
CAS	FGOALS-g3	27	Li (2019)	Li et al. (2020)	3	250 km	100 km
NOAA-GFDL	***GFDL-CM4***	28	Guo et al. (2018)	Held et al. (2019)	1	100 km	25 km
NOAA-GFDL	GFDL-ESM4	29	Krasting et al. (2018)	Dunne et al. (2020)	3	100 km	50 km
NASA-GISS	***GISS-E2-1-G (p3)***	30	GISS (2018)	Miller et al. (2021)	10	250 km	100 km
NASA-GISS	GISS-E2-1-G-CC	31	GISS (2019a)	Kelley et al. (2020), Miller et al. (2021)	1	250 km	100 km
NASA-GISS	GISS-E2-1-H (p3)	32	GISS (2019b)	Miller et al. (2021)	1	250 km	100 km
NASA-GISS	GISS-E2-2-G	33	NASA GISS (2019a)	Rind et al. (2020)	1	250 km	100 km
NASA-GISS	GISS-E2-2-H	34	NASA GISS (2019b)	Rind et al. (2020)	1	250 km	100 km
MOHC	HadGEM3-GC31-LL	35	Ridley et al. (2019a)	Andrews et al. (2020), Kuhlbrodt et al. (2018)	55	250 km	100 km
MOHC	HadGEM3-GC31-MM	36	Ridley et al. (2019b)	Andrews et al. (2020)	4	100 km	25 km
CCCR-IITM	IITM-ESM	37	Narayanasetti et al. (2019)	Krishnan et al. (2021)	1	250 km	100 km
INM	INM-CM4-8	38	Volodin et al. (2019a)	Volodin et al. (2010)	1	100 km	100 km
INM	INM-CM5-0	39	Volodin et al. (2019b)	Volodin et al. (2017), Volodin and Kostrykin (2016)	10	100 km	50 km

https://doi.org/10.5194/egusphere-2024-3057
Preprint. Discussion started: 23 October 2024

IPSL	IPSL-CM5A2-INCA	40	Sepulchre et al. (2019)	Boucher et al. (2020a)	1	500 km	250 km
IPSL	IPSL-CM6A-LR	41	Boucher et al. (2021b)	Boucher et al. (2020b)	33	250 km	100 km
IPSL	IPSL-CM6A-LR-INCA	42	Boucher et al. (2021a)	Boucher et al. (2020b)	1	250 km	100 km
NIMS-KIMA	KACE-1-0-G	43	Lee et al. (2020)	Byun et al. (2019)	2	250 km	100 km
KIOST	KIOST-ESM	44	Pak et al. (2021)	Kim et al. (2019)	1	250 km	100 km
UA	MCM-UA-1-0	45	Stouffer (2019)	Stouffer (2019)	1	250 km	250 km
MIROC	MIROC-ES2H	46	Watanabe et al. (2021)	Kawamiya et al. (2020)	30	250 km	100 km
MIROC	***MIROC6***	47	Tatebe and Watanabe (2018)	Tatebe et al. (2019)	30	500 km	100 km
MIROC	MIROC-ES2L	48	Hajima et al. (2019)	Hajima et al. (2020)	50	250 km	100 km
HAMMOZ-Consortium	MPI-ESM-1-2-HAM	49	Neubauer et al. (2019)	Neubauer et al. (2019)	3	250 km	250 km
MRI	***MRI-ESM2-0***	50	Yukimoto et al. (2019b)	Yukimoto et al. (2019a)	3	100 km	100 km
NCC	NorCPM1	51	Bethke et al. (2019)	Bethke et al. (2019)	30	250 km	100 km
NCC	***NorESM2-LM***	52	Seland et al. (2019)	Seland et al. (2020)	3	250 km	100 km
NCC	NorESM2-MM	53	Bentsen et al. (2019)	Seland et al. (2020)	3	100 km	25 km
AS-RCEC	TaiESM1	54	Lee and Liang (2020)	Wang et al. (2021)	2	100 km	100 km
MOHC	***UKESM1-0-LL***	55	Tang et al. (2019)	Sellar et al. (2019)	16	250 km	100 km
MOHC	UKESM1-1-LL	56	Walton et al. (2022)	Mulcahy et al. (2023)	1	250 km	100 km

Table 2. List of CMIP6 models used. Numbers attributed to each model are used to label each model in later figures. RAMIP models are indicated using ***bold italics***.

https://doi.org/10.5194/egusphere-2024-3057
Preprint. Discussion started: 23 October 2024

2.3 Methodology

The majority of the analysis in this study uses monthly mean outputs; while daily mean outputs are better able to capture sub-seasonal variability, these were not available for most models for variables such as speciated AOD. However, daily mean outputs are used for evaluation of daily precipitation behaviour, in order to investigate the representation of wet and dry days as well as rainfall intensity in CMIP6 models.

For the observational and reanalysis datasets used, the maximum available time domain over the 1981-2023 period is used, to minimise the influence of low-frequency variability and better capture the characteristics of the annual cycles. The available time domain is different for each dataset, as discussed below. For AOD, since part of the available reanalysis dataset is past the end date of the *historical* CMIP runs, ScenarioMIP (O'Neill et al., 2016) experiments are used, following the *SSP3-7.0* scenario. Over the timespan that this covers (2015 to 2023), the differences in emissions inventories between SSPs cause minimal differences in AOD at the continental scale for Africa (Lund et al., 2019).

The large bounding box used for this study (40°S, 40°N, 20°W, 50°E) is based on the sub-region boxes defined by the IPCC (Chen et al., 2021), covering the whole of the African continent. Areas of particular focus are the east and west African monsoon regions; both these regions feature a complex climatology with known biases, and strong future climate responses. In this study, west Africa is defined by (10°S – 15°N, 20°W – 25°E), and east Africa by (5°S – 15°N, 27°E – 46°E), as these capture the key features of the monsoon climatology.

Monthly means are used for evaluation of the annual cycle for each model. In addition, the spatial distribution of rainfall is evaluated seasonally, focusing on JJA and DJF to capture the periods of maximum northward and southward displacement of the ITCZ. For more specific regional analysis it would be preferable to instead use the relevant monsoon periods, for example over west Africa this would be JAS, as seen in Figure 12. However, using DJF and JJA was chosen for studying the performance over a larger region while still demonstrating the seasonal shifts in spatial distributions.

As discussed in Sect. 2.1.3, the CHIRPS precipitation observational dataset is only available over land. Therefore, for calculating the bias and pattern correlation associated with each model, a land mask corresponding to areas where the land mass fraction for that model was greater than 0.5 was applied.

Retrieval of $PM_{2.5}$ data was more complex; of the models for which $PM_{2.5}$ data was available, GFDL-ESM4, GISS-E2-1-G, IPSL-CM5A2-INCA, MIROC6, and NorESM2-LM output $PM_{2.5}$ directly, whilst CESM2, EC-Earth3-AerChem, UKESM1-0-LL output MMRs of 7 $PM_{2.5}$ components including sulfate (SO_4), organic carbon (OA), black carbon (BC), sea salt (SS), dust (DU), nitrate, and ammonium. The mixing ratios of $PM_{2.5}$ and its components were obtained using MMR diagnostics for the *SSP3-7.0* experiments, from 2015 to 2023.

Observed measurements of $PM_{2.5}$ in the AirNow database in Africa began in August 2016. In cases where the CMIP6 models do not provide $PM_{2.5}$ directly, we calculate it from speciated mass-mixing ratios at the surface, following Turnock et al. (2020):

$$PM_{2.5} = BC + SO_4 + OA + (0.25 \times SS) + (0.1 \times DU), \quad (1)$$

https://doi.org/10.5194/egusphere-2024-3057
Preprint. Discussion started: 23 October 2024

where *BC*, SO_4, *OA*, *SS*, and *DU* are the surface mass mixing ratios of black carbon, sulphate, organic aerosol, sea salt, and dust respectively. We computed monthly mean simulated $PM_{2.5}$ from the CMIP6 models and corresponding monthly ensemble mean surface $PM_{2.5}$ observations at each location, after all models were regridded to a common grid (1° x 1° resolution) before performing $PM_{2.5}$ calculations using the nearest available gridpoint. The performance of the models was evaluated using the coefficient of determination (R^2), root mean squared error (RMSE), and mean absolute error (MAE). All regridded data is interpolated to a 1° x 1° resolution grid unless otherwise specified.

For precipitation evaluation, pattern correlation is performed using the 2D-regridded model field compared to the 2D-regridded observational field, where both datasets are regridded to a 1°×1° grid. The same method is used to calculate the pattern correlation coefficients for the AOD, correlating against the reanalysis dataset. This calculation shows how well the pattern of modelled data matches that of the observation or reanalysis over the domain. For precipitation, this is useful since we are interested in the representation of rainfall location and progression, because this may influence aerosol-precipitation interactions and the precipitation response to regional climate forcing. Pattern correlation is also useful for AOD, as it demonstrates how well the locations and sizes of areas of high AOD are captured. However, the pattern correlation provides no indication of whether the average magnitude of rainfall or AOD is correct. Therefore, to indicate the performance of the magnitude of the fields, the RMSE is also shown for the spatial plots.

3 Results

In this section, we evaluate the performance of CMIP6 models in replicating $PM_{2.5}$, AOD, and precipitation compared to observations and reanalyses. We first start with a summary figure (Sect. 3.1), and then provide details for $PM_{2.5}$, AOD and precipitation performances.

3.1 Summary of results

An overview of the results for the evaluation of precipitation and AOD performance can be found in Figure 2. This figure provides an overview of each model's performance in non-dust and dust AOD seasonal spatial patterns, AOD climatology over east and west Africa, precipitation seasonal spatial pattern, monsoon progressions in east and west Africa (demonstrated through zonal mean precipitation climatology), and daily precipitation distributions over east and west Africa. Models that perform consistently well in seasonal spatial AOD patterns are MRI-ESM2-0 and IPSL-CM6A-LR, and these models also perform well in seasonal spatial precipitation patterns. In contrast, CESM2, CESM2-WACCM, and NorESM2-MM all perform consistently well for their precipitation patterns, but have difficulties replicating AOD patterns, particularly for dust AOD when compared to the performance of other models. These results are discussed in more detail in the relevant sections.

3.2 $PM_{2.5}$

For evaluating the behaviour of $PM_{2.5}$ in the models, the behaviour of the $PM_{2.5}$ timeseries for 12 different cities is examined. Figure 3 shows the comparison of time series of $PM_{2.5}$ in CMIP6 models and surface observations from reference monitors

https://doi.org/10.5194/egusphere-2024-3057
Preprint. Discussion started: 23 October 2024

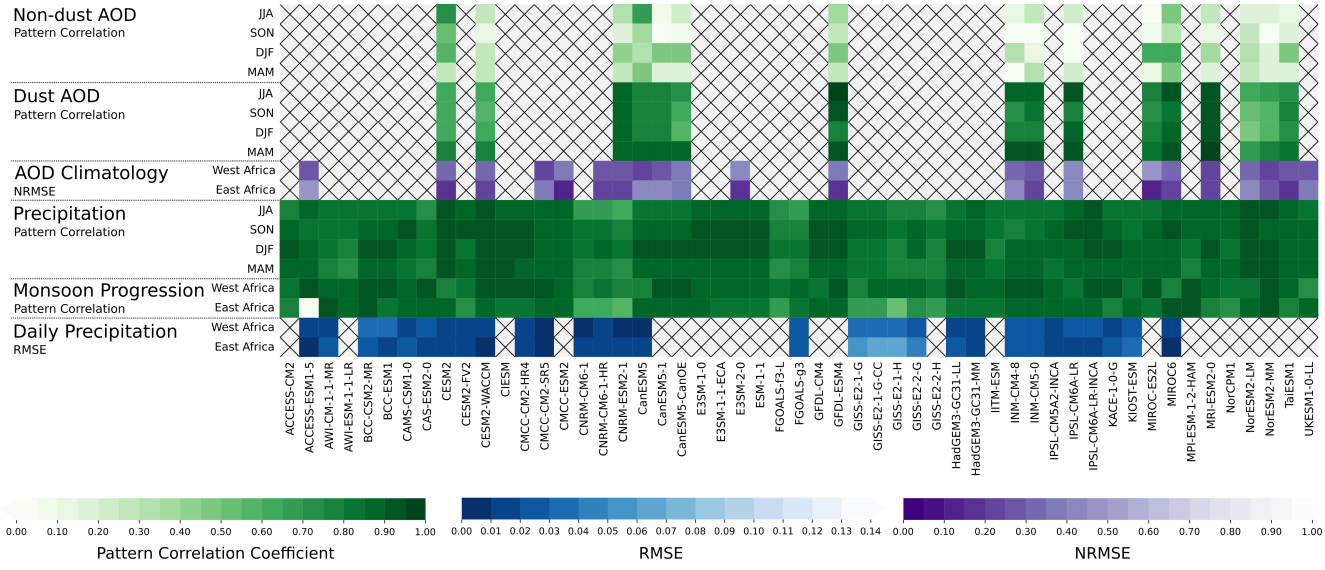

Figure 2. Performance indicators across precipitation and AOD for all models evaluated in this study. Green indicates pattern correlation coefficient, blue indicates RMSE, and purple indicates NRMSE, where more saturated colours indicate better performance for all colour scales.

at 12 U.S. Embassy locations in Africa. In this figure, the interannual variations are not expected to match with those of observations, as individual years in CMIP are not designed to correspond to the observed years. The CMIP6 models capture the seasonal cycle better in west Africa (1, 2, 3, 5, 7, 10, 12) than in east Africa (4, 8, 9, 11). This is also evident in the R^2, RMSE, and MAE values shown in Table S1. West Africa's $PM_{2.5}$ levels are largely influenced by the Harmattan season, which is associated with increased dust and a northeasterly flow over much of north Africa, carrying dust from the Sahara Desert (Anuforom, 2007). Therefore, accurate $PM_{2.5}$ simulation in a model is closely tied to its representation of atmospheric circulation and magnitude of dust emission, the latter of which differs strongly between models (Zhao et al., 2022). Conversely, east Africa's $PM_{2.5}$ concentrations are more heavily influenced by local emissions (Kalisa et al., 2023) and thus model climatologies are dependent on the accuracy of emissions inventories.

From Figure 3, it can be seen that the models demonstrate a strong diversity in magnitude for $PM_{2.5}$ concentrations. It could be expected that the modelled $PM_{2.5}$ would be too low compared to that of the observations, as the observation stations are in urban areas which are not modelled by the CMIP6 models, and as Schutgens et al. (2016) demonstrates that increasing gridbox sizes and distances from observation stations to gridpoints result in increased errors. There is a mixture of both positive and negative $PM_{2.5}$ concentration biases. CMIP6 models can be seen to generally capture the $PM_{2.5}$ annual cycle well. Cairo is a notable exception, as models underestimate $PM_{2.5}$ relative to the surface observations and do not match the observed seasonal cycle. However, there is a very small time period for which $PM_{2.5}$ observed data is available over Cairo (<1 year), and future observational data may show stronger agreement with the models. IPSL-CM5A2-INCA overestimates surface $PM_{2.5}$

https://doi.org/10.5194/egusphere-2024-3057
Preprint. Discussion started: 23 October 2024

observations in all locations, especially during periods of increased $PM_{2.5}$ levels. This may relate to biases in daily precipitation behaviour, as IPSL-CM5A2-INCA underestimates the upper end of daily rainfall amounts in both east and west Africa — daily precipitation behaviour is discussed further in Sect. 3.4.3. However, MIROC6 displays similar behaviour in daily precipitation to IPSL-CM5A2-INCA, and yet has the opposite bias; MIROC6 underestimates $PM_{2.5}$ at most observation stations. However, MIROC6, despite underestimating the upper end of daily rainfall, exhibits wet biases for most seasons over much of Africa, especially west Africa, where biases in IPSL-CM5A2-INCA for the same region are less clear.

Most models perform best in Accra, Ouagadougou, Abidjan, Abuja, and Lome with R^2 ranging from 0.35 to 0.96 and mean absolute error (MAE) ranging from 2.42 μgm^{-3} to 20.07 μgm^{-3}. All the models perform poorly in Kampala, Nairobi, Kigali, Addis Ababa, Bamako, and Dakar, with the largest RMSE and MAE in Bamako, ranging from 26.91 μgm^{-3} to 31.44 μgm^{-3} and 22.01 μgm^{-3} to 25.07 μgm^{-3} respectively. It is noticeable that the cities with poor performance are generally located in east Africa, with the exception of Bamako and Dakar. This is in agreement with results for the larger scale AOD analysis in shown later in Sect. 3.3, where representation of the annual cycle of AOD is found to be generally poorer over east Africa compared to west Africa. In addition, the complex monsoon climatology impacts the levels of $PM_{2.5}$, and so poorer performance in simulating the EAM compared to the WAM, discussed in Sect. 3.4.2 and Sect. 3.4.1, may be related to some models' struggles at replicating $PM_{2.5}$ concentrations over the region.

3.3 Aerosol Optical Depth

For evaluating the behaviour of AOD in the models, we consider the accuracy of both dust and non-dust AOD distributions separately, as they have different contributions of uncertainty and separate analysis makes the origins of biases easier to identify. We also examine the accuracy of the seasonal cycle of AOD over subregions in Africa.

The key results of AOD evaluation can be seen in Figure 4 and Figure 5. They show the reanalysis (CAMS) distribution of dust and non-dust AOD during SON, the MMM, the intermodel standard deviation, the bias in the MMM, and the biases in the models with the least and most deviation from the spatial pattern of dust and non-dust AOD in CAMS. SON is used as the example season for the AOD analysis, as it shows the strongest intermodel diversity, and lowest overall performance for both the dust and non-dust AODs.

Figure 4 shows that the MMM, while generally in agreement with reanalysis, does not fully capture the distribution of dust AOD during SON. The northward and westward extent of the high dust AOD over the Sahara is not well captured, with a positive bias over northeast Africa, and a negative bias over the northwest. Strong intermodel variability over the central Saharan region is likely to be due to differences in the simulation of dust emissions — many CMIP6 generation models calculate dust emissions interactively, so there are strong differences in the magnitude of dust aerosol.

The closest model to the reanalysis, GFDL-ESM4, captures the dust AOD well. While the biases that are present still show a negative (postive) dust AOD bias over northwest (northeast) Africa, the model performs well overall for SON, with a pattern correlation of 0.95 and a RMSE of 0.04.

The model furthest from the reanalysis, NorESM2-LM, has a positive bias in dust AOD of >0.8 over northeast Africa extending into central Africa and a strong negative bias over northwest Africa, as well as a positive AOD bias over southern

https://doi.org/10.5194/egusphere-2024-3057
Preprint. Discussion started: 23 October 2024

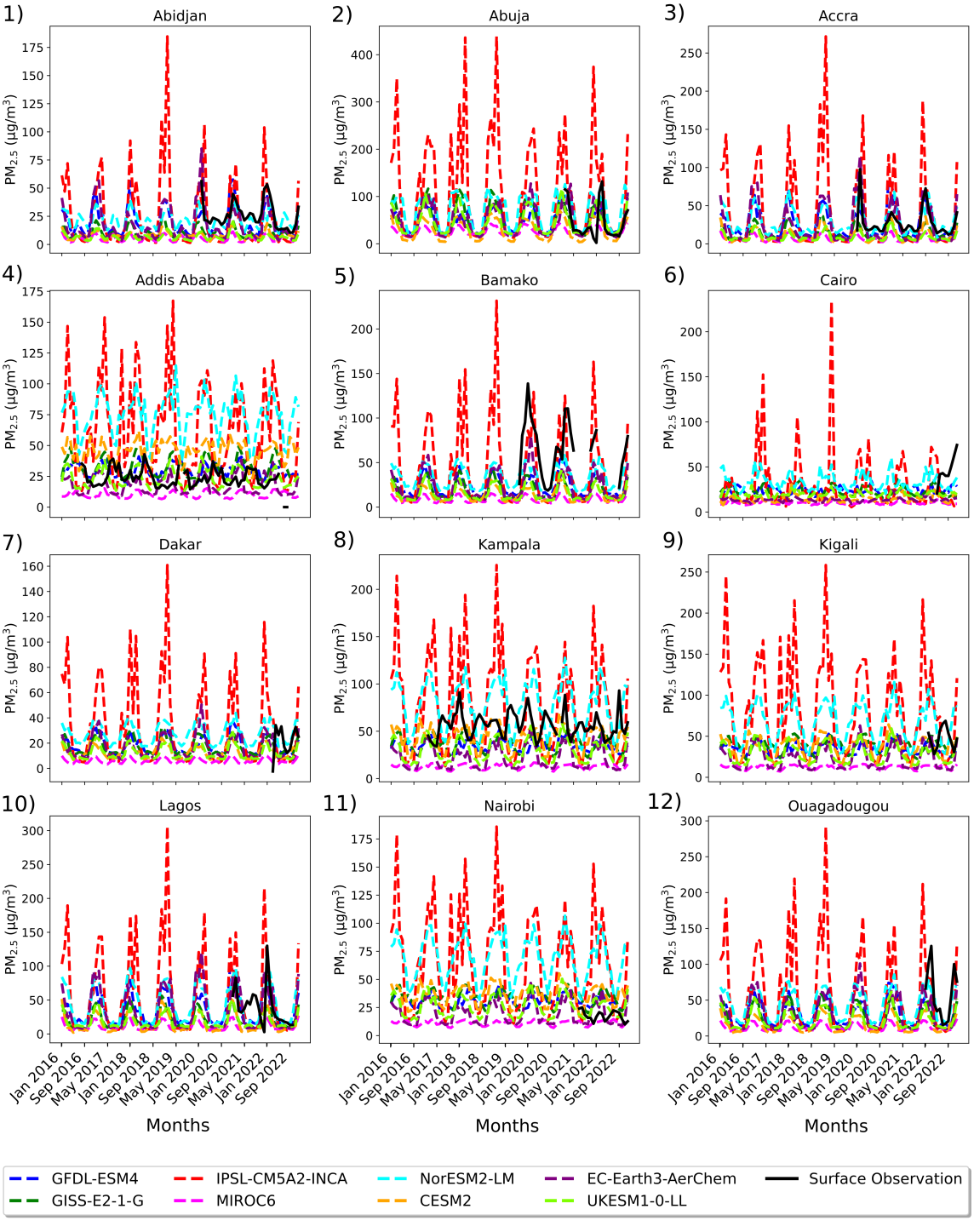

Figure 3. Comparison of CMIP6 models (dashed coloured lines) and surface $PM_{2.5}$ observations (solid black lines) with reference monitors at U.S. embassy locations in Africa. Note changing y-axis between plots. A common x-axis is used, though not all of the dates are covered for each location by the available observational dataset. Numbers refer to station locations mapped in Figure 1 and detailed in Table 1. Units are $\mu g m^{-3}$.

https://doi.org/10.5194/egusphere-2024-3057
Preprint. Discussion started: 23 October 2024

Africa. The latitudinal band of maximum AOD also shows a southward bias. NorESM2-LM is in the CESM2 family of CMIP6 models (CESM2, CESM2-FV2, NorESM2-MM, etc.), which tend to produce the correct amount of dust, but confine it to only a small number of grid points (Zhao et al., 2022). This causes a common bias in these models, where the dust AOD over those areas is too high, and the AOD elsewhere in dust-affected regions is too low, which is found in this analysis in the area of positive dust AOD bias over northwest Africa. Overall this model struggles to replicate the pattern of dust AOD over Africa during SON, which is reflected in its lower pattern correlation coefficient of 0.52 and RMSE of 0.15.

Dust AOD spatial distribution over Africa in SON is well captured by most climate models. The strongest biases relate to the area of high dust AOD over the Sahara being too far eastward, and the magnitude of peak AOD being overestimated.

For non-dust AOD, Figure 5 shows that the MMM does not capture the distribution of non-dust AOD during SON well. The MMM and MMM bias in Figure 5b and 5c show a positive AOD bias over the west coast of west Africa, which may be due to coincident anomalous westerly winds. As these act to weaken the south easterly flow from over the Gulf of Guinea, less clean air is advected, which may lead to the positive AOD bias. The area of high AOD over southern central Africa, associated with biomass burning, is missing from the MMM.

The closest model to the reanalysis, CESM2, captures some of the non-dust AOD spatial pattern. The negative AOD bias found in the MMM over southern central Africa is still present, though biases elsewhere are reduced. It is notable that the CESM2 model family that performed poorly for the dust AOD pattern, performs best in the non-dust AOD pattern evaluation, though none of the models analysed produce non-dust AOD similar to that of the reanalysis. CESM2 is found to have a pattern correlation of 0.50 and a RMSE of 0.08.

For the model furthest from the reanalysis, CanESM5-1, the negative AOD bias found in the MMM over southern central Africa is present. In addition, a strong positive (> 0.8) AOD bias is found over UAE — this AOD bias covers a large area north-eastward and is not limited to Africa. CanESM5-1 was found to have a negligible pattern correlation coefficient of -0.08 and an RMSE of 0.25.

Non-dust AOD spatial distribution over Africa in SON is not well captured by the climate models analyzed here. The strongest bias relates to a negative AOD anomaly found over southern central Africa.

Figure 6 shows the comparative performance of the models when ranked by pattern correlation compared to CAMS for each season, with RAMIP models highlighted in red, for dust AOD and non-dust AOD. The mean performance of the CMIP6 models is lowest in DJF for the dust AOD, and in SON for the non-dust AOD. For the dust AOD, this coincides with the Harmattan season which occurs in NDJFM. Reduced performance during the DJF season may indicate that CMIP6 models are struggling to replicate the seasonal cycle of circulation, and associated dust changes in the Harmattan season. Poor performance in the Harmattan season makes projections of changes in air quality, especially extreme air quality events, from the CMIP6 ensemble less reliable. For the non-dust AOD, SON is associated with biomass burning in central Africa, where the strong negative bias is seen in all of the models. Emissions inventories may not be capturing the magnitude of biomass burning emissions over the central African region during SON, as current literature notes underestimates of AOD increases in southern Africa (Lund et al., 2023).

https://doi.org/10.5194/egusphere-2024-3057
Preprint. Discussion started: 23 October 2024

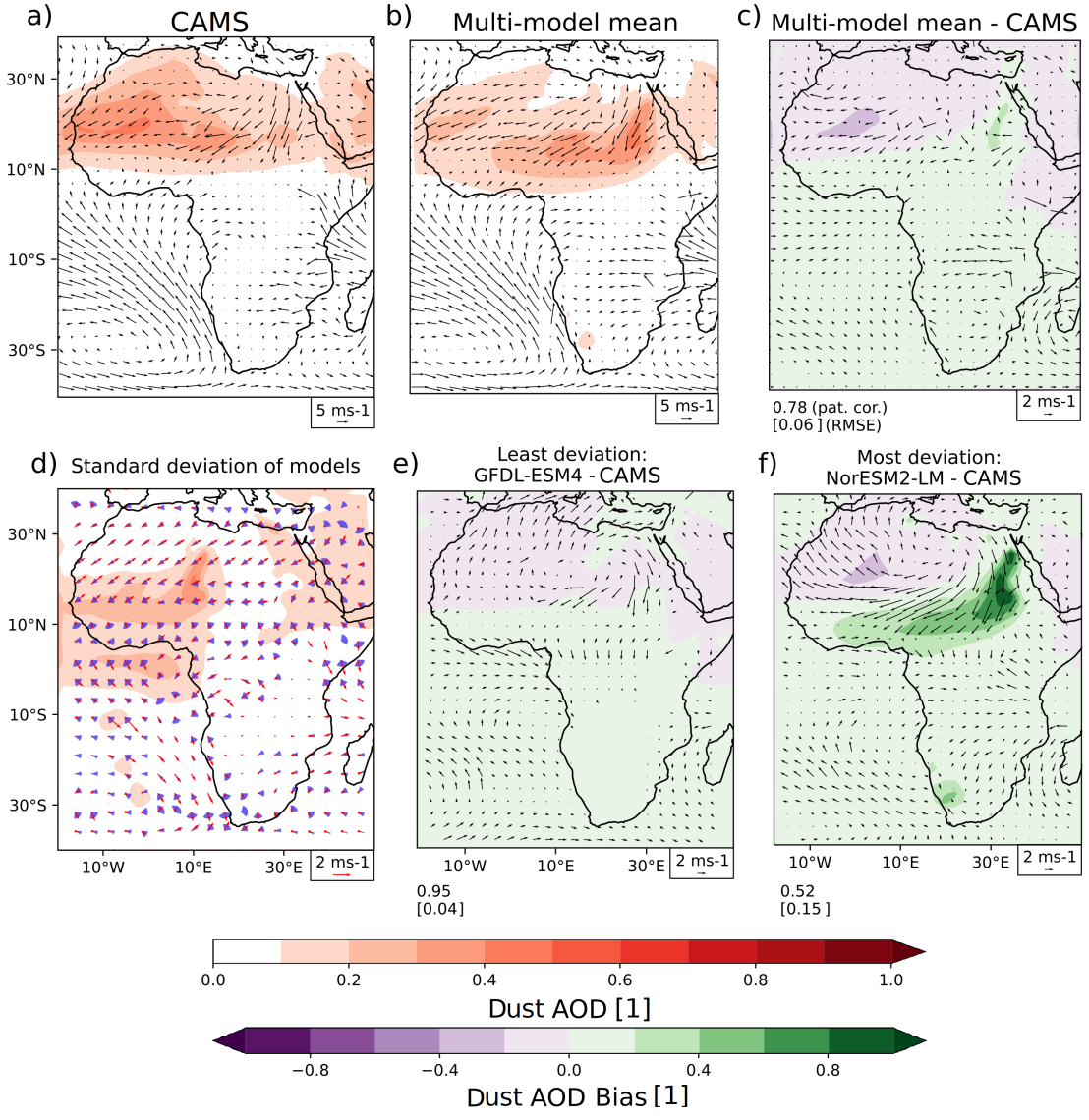

Figure 4. SON-mean dust AOD and lower-tropospheric (925 hPa) winds for 2002–2023 in (a) observations (CAMS/ERA5) and (b) CMIP6 MMM. (c) CMIP6 MMM bias against observations and (d) intermodel standard deviation for precipitation (shading) and wind speed along the mean wind direction (red) and wind direction (blue). Mean dust AOD and wind fields in the models with the (e) least (GFDL-ESM4) and (f) most (NorESM2-LM) deviation from CAMS as determined by pattern correlation. Pattern correlation and RMSE compared to CAMS are shown below panels (c), (e), and (f). Note that the reference vectors for the 925 hPa winds differ between panels.

https://doi.org/10.5194/egusphere-2024-3057
Preprint. Discussion started: 23 October 2024

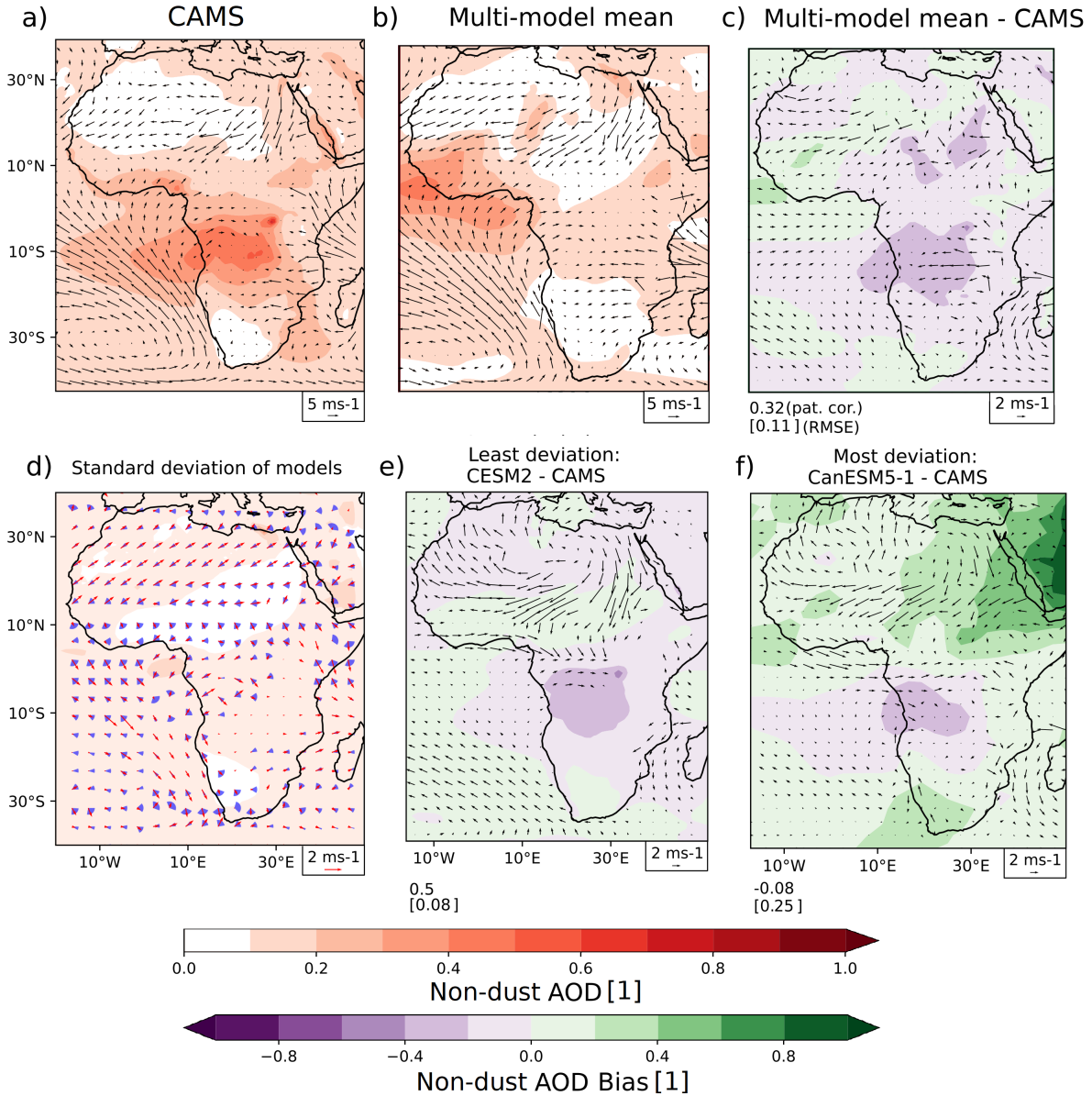

Figure 5. Same as Figure 4, but for non-dust AOD. The model with the least deviation from CAMS is now CESM2, and the model with the most deviation from CAMS is now CanESM5-1.

https://doi.org/10.5194/egusphere-2024-3057
Preprint. Discussion started: 23 October 2024

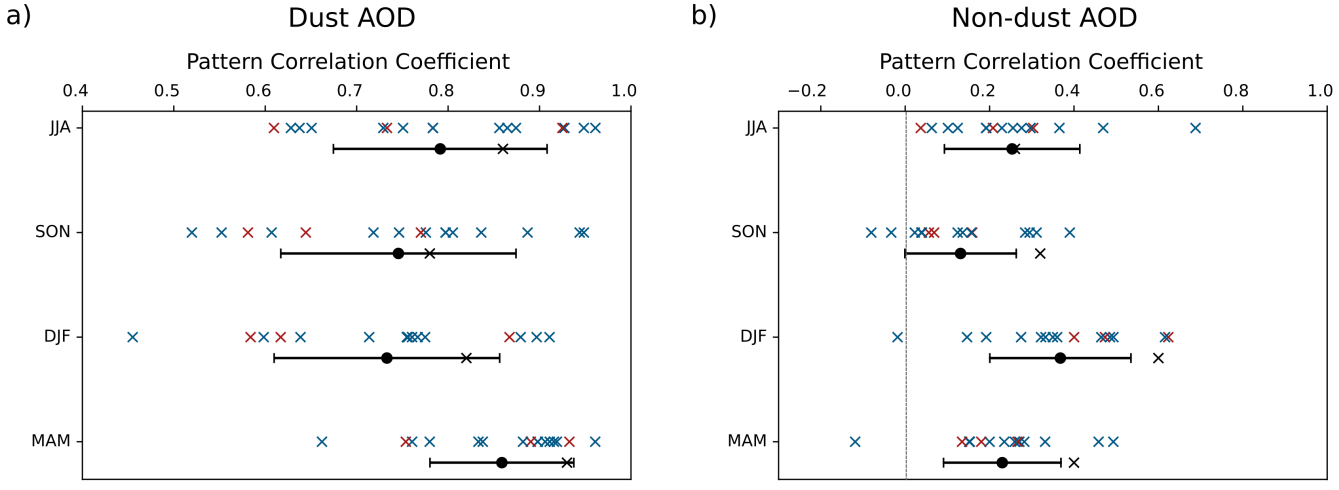

Figure 6. Models ranked by pattern correlation for seasonal (a) dust AOD and (b) non-dust AOD over Africa (40°S – 40°N, 20°E – 50°E), with the RAMIP models highlighted in red. Black dot shows the mean of the individual model pattern correlation coefficients, black cross shows the MMM pattern correlation coefficient, and the whiskers show the standard deviation of the model pattern correlation coefficients. Evaluation is performed using CAMS over the time period 2002-2023.

Inaccuracies in emissions inventories may be the cause of poorer performance for non-dust AOD over Africa. However, there is higher diversity in the pattern correlation coefficients for non-dust aerosol. Therefore, differences in the treatment of aerosols by different models still drives strong intermodel diversity even for prescribed aerosol emissions.

3.3.1 West African AOD Climatology

Different regions in Africa are characterized by different AOD climatologies according to relevant emissions and local meteorology, with consequences for human health and local climate. Understanding the impacts of evolving aerosol emissions is reliant on accurate interactions of the emissions with the meteorology of their source regions.

The normalized root mean square error (NRMSE) is used to rank model performance from least deviation (lowest NRMSE) to most deviation (highest NRMSE).

Figure 7 shows the seasonal cycle of AOD over west Africa in the reanalysis (CAMS), MMM, the model with the lowest NRMSE (MRI-ESM2-0), and model with the highest NRMSE (MIROC-ES2L). The interannual variability of the seasonal cycle is shown through shading.

In Figure 7a, AOD can be seen to have two peaks in west Africa in February-March and JJA. This climatology is driven by seasonal winds bringing dust from the Sahara, local aerosol emission annual cycles, and monsoon seasons of high rainfall reducing AOD. The peak in DJFM is due to Harmattan winds bringing dry dusty air from the Sahara, while Senghor et al. (2017) links the peak in JJA AOD to transport from coastal sand sources. For the interannual variability, higher variability is

https://doi.org/10.5194/egusphere-2024-3057
Preprint. Discussion started: 23 October 2024

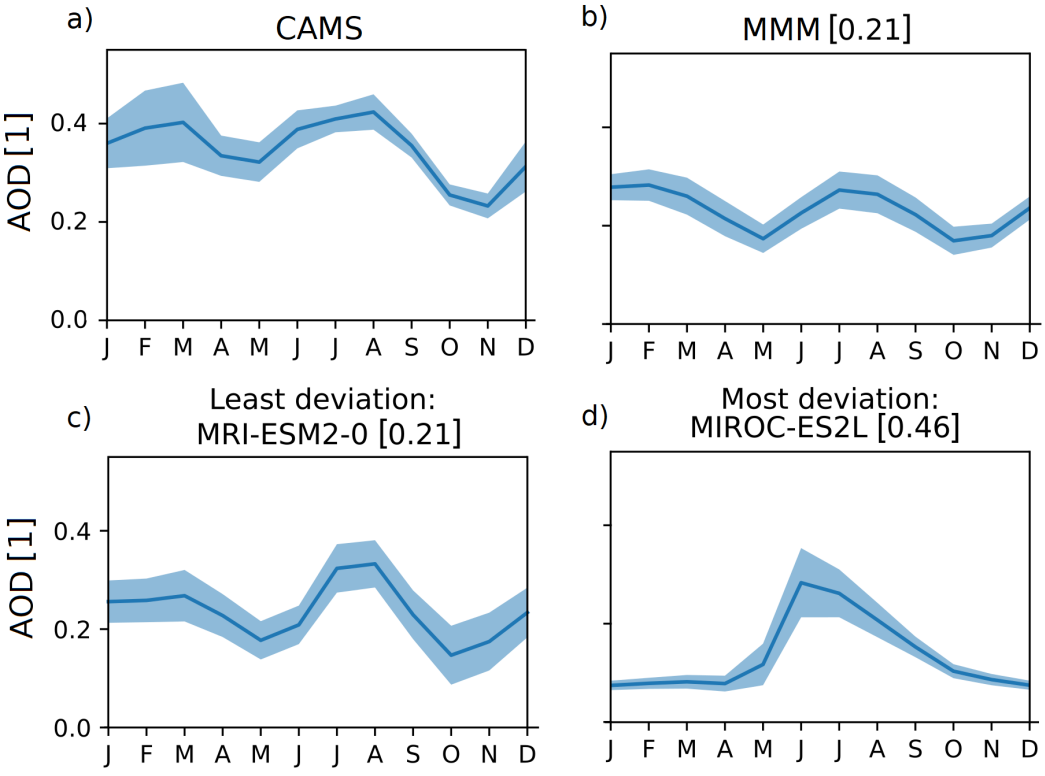

Figure 7. Monthly mean total AOD over west Africa (10°S – 15°N, 20°W – 25°E) for (a) reanalysis (CAMS), (b) MMM, (c) the models with the lowest NRMSE (MRI-ESM2-0), and (d) the highest NRMSE (MIROC-ES2L), with NRMSEs against CAMS shown in square brackets. Interannual standard deviation for each month is shown in shading. Evaluation is performed using CAMS over the time period 2002-2023.

noticeable during the Harmattan season, DJFM, which stems from differing strength of the Harmattan winds interannually — this can be seen in the high standard deviation of lower-tropospheric wind speed during DJFM compared to the rest of the year.

The MMM shown in Figure 7b shows the two peaks, though there are issues with the timing of the peaks; the first peak occurs too early by one month. The change in interannual variability in AOD through the year is not captured either, so the variability of the Harmattan season is not captured. Overall, the MMM captures the pattern of AOD climatology to first order, though it does not correctly capture the timing of the AOD peaks, and does not capture the changes in variability through the year.

The model with the lowest NRMSE, MRI-ESM2-0, better captures the distinct traits of the AOD peaks in each season. There are still issues with the timing of the peaks — while the first peak occurs at the right time, the second peak is too late, and at least a month too short. In addition, the variability is similar year round, with a slight increase in October-November, which is the opposite of the variability seen in CAMS. These biases could originate from issues with capturing interannual variability of the Harmattan season, as the zonal mean precipitation climatology is found to be accurate, with only small wet biases during

https://doi.org/10.5194/egusphere-2024-3057
Preprint. Discussion started: 23 October 2024

MAM. Examining the interannual standard deviation in seasonal wind speed over Africa in MRI-ESM2-0 shows that, while capturing some increases in variability during DJF, the area of increased variability is too small, and the increase is too weak to fully capture the Harmattan and its effects.

The model with the highest NRMSE, MIROC-ES2L, does not capture the two-peaked climatology at all, instead having a single AOD peak in June-July. In addition, the variability in this model is strongest in the June-July period, and is minimal elsewhere. This could relate to issues in the precipitation distribution, as MIROC-ES2L is found to have strong wet biases over west Africa — if a model has too many wet days the lifetime of aerosol can be drastically reduced due to excessive scavenging, causing a low bias in AOD. The latitudinal progression of rainfall in MIROC-ES2L shows a strong wet bias in JAS, but the modelled AOD is most accurate during JAS, and so there are no obvious parallels between poor performance in both the AOD and the zonal mean precipitation climatology.

Overall, the general pattern of AOD climatology throughout the year is captured, though there are some issues with timing of peak AOD. Interannual variability in AOD associated with the Harmattan season is not well captured in the MMM or the best performing model. These issues with AOD climatology could be related to the biases in circulation (particularly the Harmattan winds which cause the DJFM AOD peak) and precipitation behaviour over the region, particularly biases in the number of wet days per year.

3.3.2 East African AOD Climatology

Figure 8 shows the climatology of AOD over east Africa in the reanalysis dataset, CAMS, the AOD climatology of the MMM, and the AOD climatologies of the models with the lowest and highest NRMSE.

In Figure 8a, the AOD climatology characteristics differ greatly to that of west Africa. Dust from the Sahara desert is not as dominant as for west Africa, and interannual variability is reduced. The AOD can be seen to have one main peak in JJA. This is due to increased positive zonal wind speed during JJA, with westeries bringing in pollution from central Africa, compared to the rest of the year in which increased easterly winds bring cleaner air from over oceans (Hastenrath et al., 2011). For the interannual variability, there is little change during the year.

From Figure 8b, the MMM can be seen to match this pattern poorly — the JJA peak in AOD is not well produced, and instead the models simulate a two-peaked climatology, more similar to that of west Africa. The variability remains constant throughout the year, similarly to the reanalysis.

The model with the lowest NRMSE, MPI-ESM1-2-HR, represents the AOD climatology more accurately than the MMM. It features the strong peak in AOD during JJA, though this peak lags a month behind that of CAMS — similar to the zonal mean precipitation cycle (Sect. 3.4.1) of the model — and has a lower peak magnitude.

The model with the highest NRMSE, ACCESS-ESM1-5, has two peaks and fails to capture the strength of the AOD peak in JJA, as well as the length of this peak, which may relate to wet biases found in the zonal mean precipitation climatology for ACCESS-ESM1-5, which are strongest in SON. In addition, the zonal mean precipitation lags behind the observations by a month for this model, which may explain negative biases after the long rains season. The variability for ACCESS-ESM1-5 is much lower than that of CAMS.

https://doi.org/10.5194/egusphere-2024-3057
Preprint. Discussion started: 23 October 2024

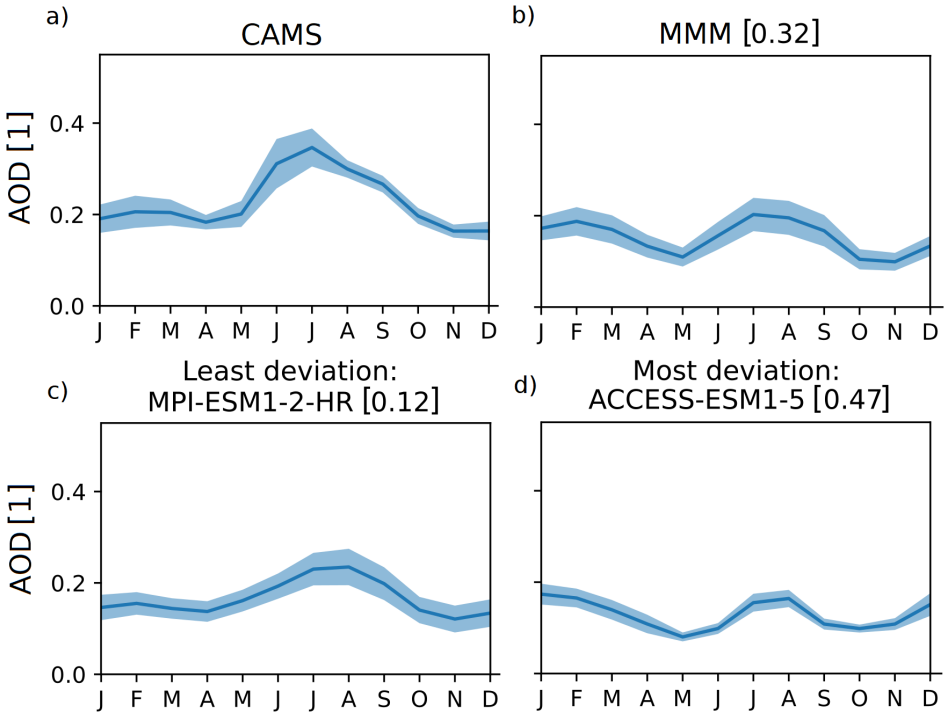

Figure 8. Monthly mean total AOD over east Africa (5°S – 15°N, 27°E – 46°E) for (a) reanalysis (CAMS), (b) MMM, (c) the models with the lowest NRMSE (MPI-ESM1-2-HR), and (d) the highest NRMSE (ACCESS-ESM1-5), with NRMSEs against CAMS shown in square brackets. Interannual standard deviation for each month is shown in shading. Evaluation is performed using CAMS over the time period 2002-2023.

395 The climatology of AOD over east Africa is less well represented than of that over west Africa, with the MMM failing the capture the AOD climatology found in the reanalysis. Variability here is better represented than of that over west Africa. Biases over east Africa are found to relate to biases in the zonal mean precipitation cycle, and may also relate to difficulties with circulation over the region, as this governs much of the seasonal cycle of AOD over east Africa.

3.4 Precipitation

400 For the observational uncertainty, African precipitation observational and reanalysis datasets demonstrate strong agreement over south and west Africa (Ayugi et al., 2024; Karypidou et al., 2022), though there are disagreements in precipitation climatology over east Africa, and some differences in the behaviour of daily precipitation (Sylla et al., 2013). Difficulties in constraining precipitation observational uncertainties over east Africa are mainly due to a scarcity of rain gauge observations (Dinku et al., 2018). An example of the diversity in east African rainfall climatology is shown in Figure 9, through the latitude-
405 time progression of the east African monsoon. It can be seen that the observational datasets disagree over both the northward

https://doi.org/10.5194/egusphere-2024-3057
Preprint. Discussion started: 23 October 2024

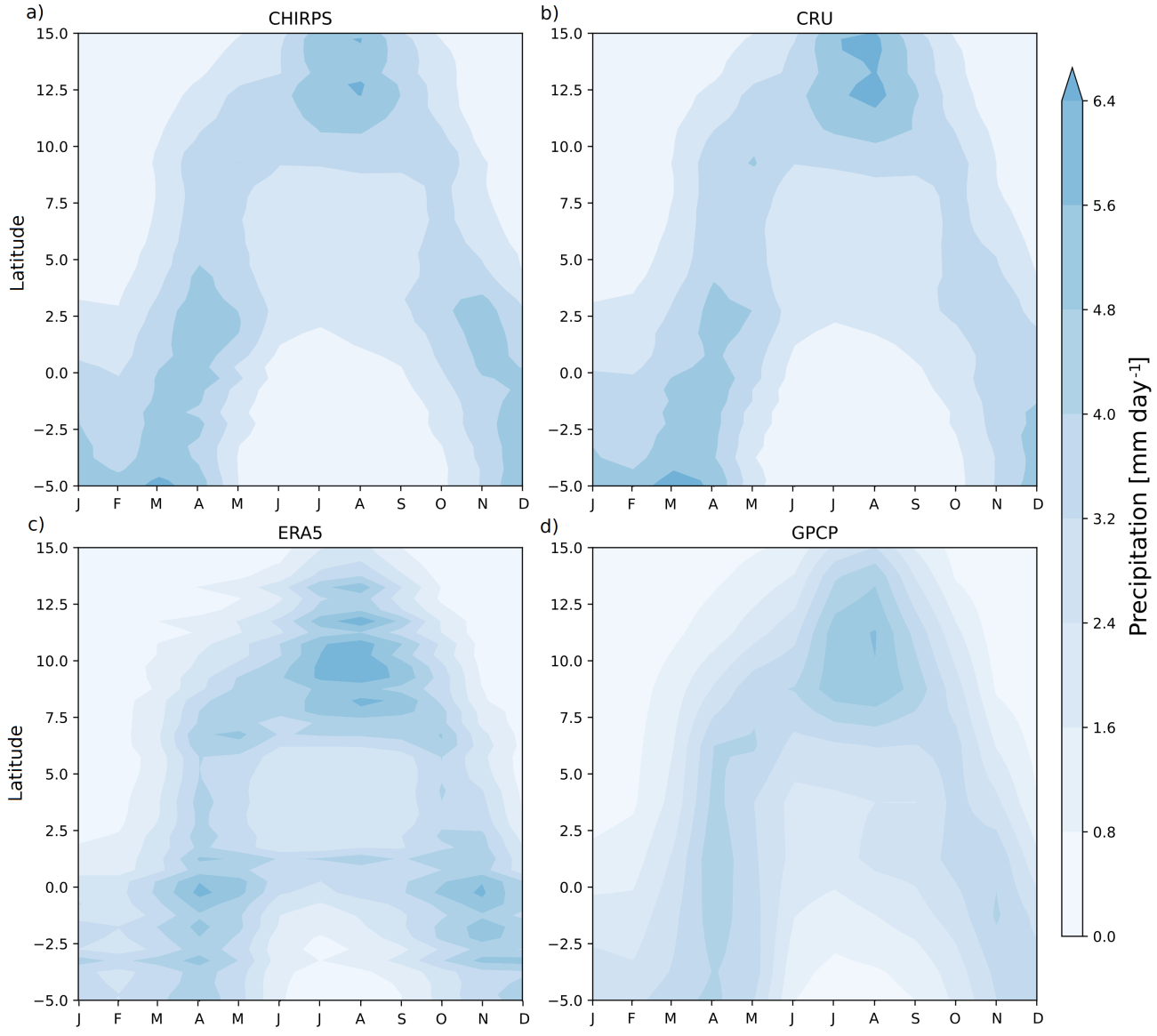

Figure 9. Observational estimates of precipitation in time-latitude diagrams of the tropical rainbelt over east Africa for the (a) CHIRPS, (b) CRU, (c) ERA5, and (d) GPCP datasets over 1981-2023. The bounding box (5°S – 15°N, 27°E – 46°E) is used. Units are mm day^{-1}.

https://doi.org/10.5194/egusphere-2024-3057
Preprint. Discussion started: 23 October 2024

extent and magnitude of mean rainfall over the region, though the annual cycle itself is consistent — the banded appearance of the ERA5 dataset is due to small hotspots of precipitation over east Africa caused by local orography. Precipitation over the majority of Africa in CHIRPS has been found to be reliable (Dinku et al., 2018), however, model performance over east Africa should be evaluated in the context of the observational uncertainty.

Figure 10 shows the observational distribution of rainfall during JJA from CHIRPS, as well as the lower-tropospheric winds from ERA5, the CMIP6 multi-model mean (MMM), the intermodel standard deviation, the bias in the MMM relative to CHIRPS, and the biases in the models with the least and most deviation from the rainfall in CHIRPS, based on a pattern correlation approach. JJA is used as the example season for the precipitation analysis, as it shows the strongest intermodel diversity, and lowest overall performance.

The most prominent feature seen in Figure 10 is the ITCZ: the region of intense rainfall centred around 10°N in JJA. Capturing the seasonal and interannual position changes of the ITCZ is important over Africa, as it has a strong influence on both the WAM and EAM. Historically, sustained equatorward shifts in the northward extent of the ITCZ caused by remote aerosol emission changes have led to strong droughts over the west African region (Monerie et al., 2023). Therefore, capturing the correct position and inland extent of the ITCZ for each season is highly important.

Figure 10 shows that rainfall biases in JJA are largely confined to the region associated with the ITCZ — it can also be seen that these are the areas of the largest intermodel spread. Though the MMM captures the magnitude and eastward extent of the WAM well, there is a southward bias in the ITCZ over west Africa, a well-known bias that has persisted over generations of CMIP models (Bock et al., 2020); the continued presence of this bias in CMIP3, CMIP5, CMIP6, and moreover in HighResMIP experiments demonstrates that increasing model resolution in parameterized models does not remove this bias. The wind biases for the MMM in Figure 10 show that the Saharan heat low (SHL) has a small ($< 5°$) southward bias. The SHL impacts the intensity and location of the WAM (Lavaysse et al., 2016). Therefore, this could be a cause of the southward bias in the WAM.

In the MMM during JJA, west Africa generally exhibits stronger biases than east Africa, with localised areas of wet biases such as over Nigeria and Gabon. In the MMM a dry bias and hot spot of large intermodel spread can be seen over Ethiopia. This is over the Ethiopian highlands, and may be due to orographical effects of the region not being captured, because of low resolution limiting the area of high elevation.

The models analyzed are found to perform well over the whole of Africa in JJA. Pattern correlations are found to be high for the MMM at 0.85, though there are some biases in the location of rainfall, and magnitude of rainfall in regions.

The model with the least deviation from CHIRPS, NorESM2-LM, shows little bias in the position of the ITCZ during JJA, and some small areas of localized biases over east Africa. While still showing a southward bias in the position of the SHL, the spatial pattern of the WAM is well captured.

The model with the greatest deviation from CHIRPS, FGOALS-g3, shows a strong bias in the position of the ITCZ over west Africa, and a strong underestimation of rainfall over central and east Africa, which may be associated with poor simulation of the ITCZ. The SHL in this model also appears to be too weak, with easterly biases in wind direction on the eastern flank of the SHL. Southward biases in rainfall over east Africa are also seen.

https://doi.org/10.5194/egusphere-2024-3057
Preprint. Discussion started: 23 October 2024

Overall, Figure 10 shows that there are large differences in the ability of the CMIP6 models to replicate African rainfall in JJA especially over west Africa and Ethiopia. The strongest intermodel spread is found over west Africa, though biases in rainfall location are found over both east and west Africa. These biases can mainly be attributed to differences in the location and strength of the ITCZ and SHL during this season.

Figure 11 shows a ranking of the pattern correlations of each of the models evaluated for each season. The season associated with the weakest overall model performance, and highest intermodel spread, is JJA, typically associated with high rainfall over west Africa. Despite having the weakest seasonal performance, the mean of the model pattern correlations for JJA is 0.83, and the multi-model mean pattern correlation is 0.85. A large number of models closer to the observations belong to the CESM family, indicating that these models perform well in simulating west African rainfall.

Figure 11 also shows the model performance during SON, DJF, and MAM. The other seasons exhibit lower intermodel spread in pattern correlation, and stronger overall performance. For the equinoctal seasons, the model performance is slightly better than in JJA, with a mean of 0.87 for SON, 0.85 for MAM. For DJF, performance overall is also better than JJA, with a pattern correlation of 0.88.

For all seasons, there is a steep drop-off in model skill for the more poorly performing models that is most pronounced in the solstitial seasons. The decline in model skill for select models during these seasons may indicate issues capturing the northward and southward extents of the ITCZ during JJA and DJF respectively. Understanding where the biases in poorly performing models originate is integral to making decisions on using their results in future projections.

3.4.1 West African Monsoon

Capturing the meridional progression of the monsoons is important for confidence in forecasts and climate projections for Africa. The progression is characterised by key monsoon characteristics, such as onset, duration, demise, and intensity, which are important to agricultural practices. The progression of the monsoon is dependent on the behaviours of several circulation systems, such as the ITCZ, tropical easterly jet, African easterly jet, and sub-tropical westerly jet (Niang et al., 2020). Poor performance in replicating the evolution of the monsoon through the year can point to difficulties in the representation of these key circulation features. In addition, over west Africa in particular, the progression of the monsoon is dependent on local features, such as soil moisture gradients, so poor performance in the monsoon climatology can point to inaccuracy in local climate factors.

The latitudinal progression of the WAM through the year is shown in Figure 12. The WAM is well captured, with a pattern correlation of 0.94 for the MMM, and with individual models having patterns correlations in the range 0.74–0.95. The temporal evolution of precipitation is well captured by the MMM, though there is an overall dry bias, as well a $\sim 4^{\circ}$ southward bias in the peak rainfall (found through the difference in the latitudes of highest rainfall).

The model with the highest pattern correlation, INM-CM4-8, underestimates the overall magnitude of rainfall, with a higher RMSE than the MMM, but captures the overall progression well, despite the southward bias in peak rainfall. The progression of intensity of the rainband for INM-CM4-8 lags behind that of CHIRPS, showing the strongest precipitation in October-

https://doi.org/10.5194/egusphere-2024-3057
Preprint. Discussion started: 23 October 2024

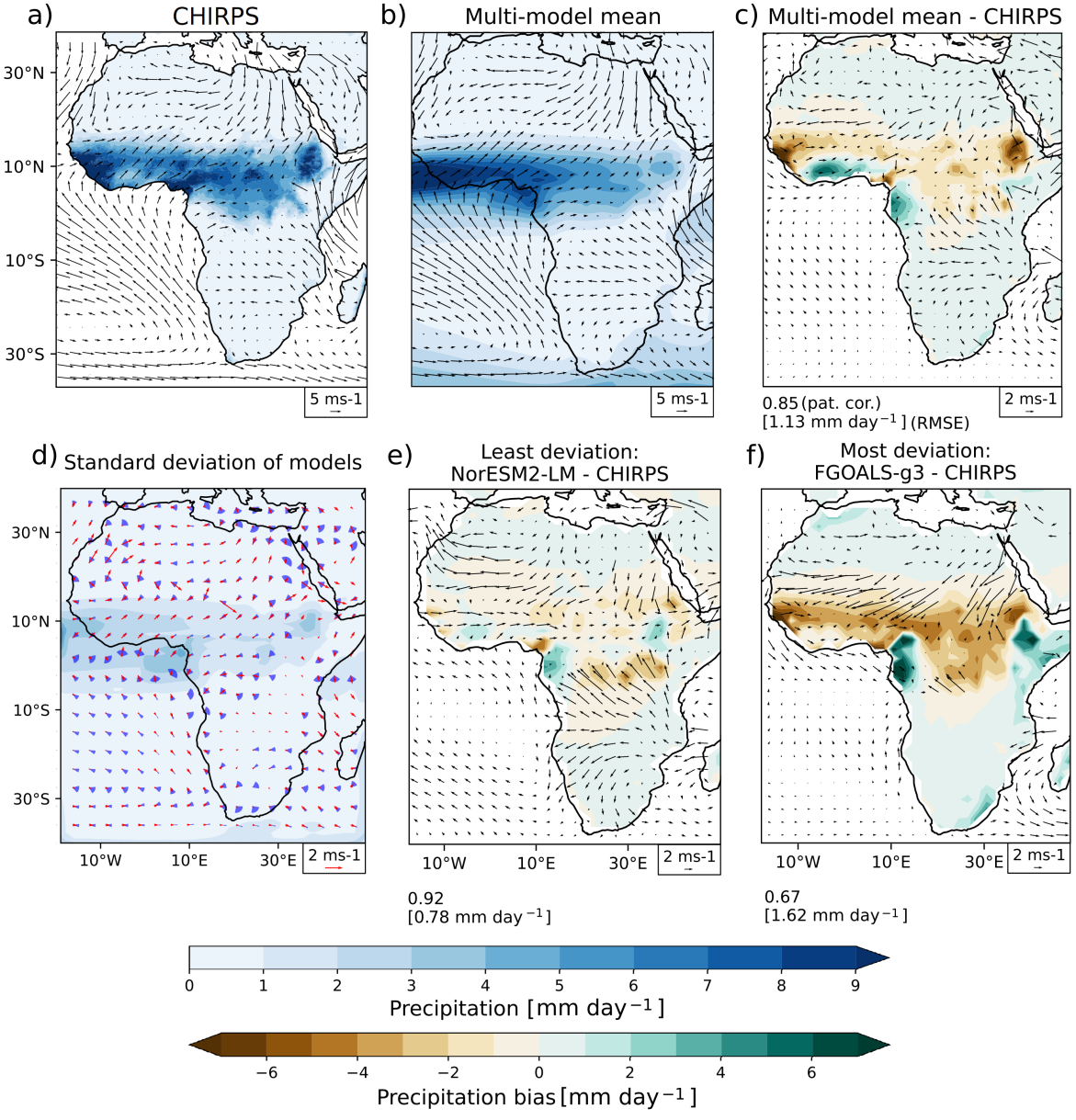

Figure 10. JJA-mean rainfall and lower-tropospheric (925 hPa) winds for 1981–2023 in (a) observations (CHIRPS/ERA5) and (b) CMIP6 MMM. (c) CMIP6 MMM bias against observations and (d) intermodel standard deviation for precipitation (shading) and wind speed along the mean wind direction (red) and wind direction (blue). Mean rainfall and wind fields in the models with the (e) least (NorESM2-LM) and (f) most (FGOALS-g3) deviation from CHIRPS as determined by pattern correlation. Pattern correlation and RMSE compared to CHIRPS are shown below panels (c), (e), and (f). Note that the reference vectors for the 925 hPa winds differ between panels.

https://doi.org/10.5194/egusphere-2024-3057
Preprint. Discussion started: 23 October 2024

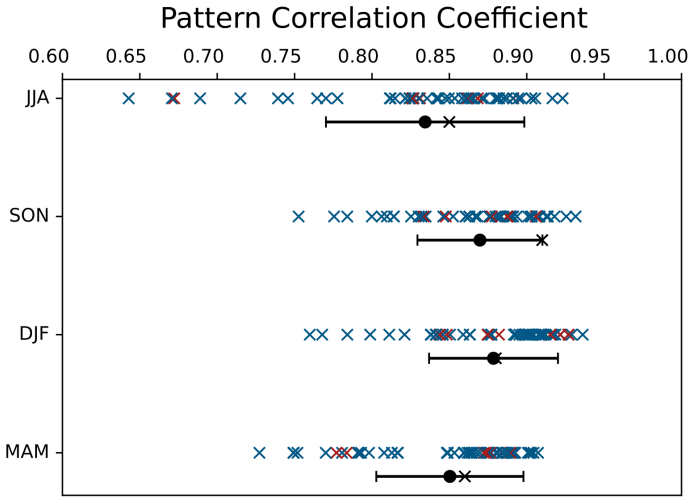

Figure 11. Models ranked by pattern correlation for seasonal rainfall over Africa (40°S – 40°N, 20°E – 50°E), with the RAMIP models highlighted in red. Black dot shows the mean of the individual model pattern correlation coefficients, black cross shows the MMM pattern correlation coefficient, and the whiskers show the standard deviation of the model pattern correlation coefficients. Evaluation is performed using CHIRPS over the time period 1981-2023.

November. No obvious relationships are found between the zonal mean precipitation shown here and AOD climatology, as the INM-CM4-8 AOD over west Africa is found to show a negative bias in AOD throughout the year.

The model with the strongest deviations from observations, UKESM1-0-LL, struggles to replicate the monsoon pattern over west Africa. This model shows the strongest rainfall for the region during MAM, much earlier than the peak in CHIRPS in August, which coincides with a negative bias in AOD over West Africa during MAM — potentially due to increased rates of wet deposition. In addition, the rainband becomes extremely weak in DJF compared to CHIRPS. This may contribute to the positive biases in AOD in UKESM1-0-LL over west Africa in DJF. The southward bias in the latitudinal location of peak rainfall is similar to that of the MMM. These biases may indicate difficulties with UKESM1-0-LL capturing the mechanisms governing the local monsoon evolution.

Overall, the WAM is well represented, especially in the MMM, despite a consistent southward bias, and overall agreement in the temporal rainfall pattern with CHIRPS indicates that the mechanisms governing the latitudinal progression of the monsoon are also well represented by the majority of models.

3.4.2 East African Monsoon

The east African monsoon has received renewed attention due to ongoing severe droughts (World Health Organisation, 2024); simulating the east African monsoon is of no less importance than in west Africa and thus monitoring and predicting changes

https://doi.org/10.5194/egusphere-2024-3057
Preprint. Discussion started: 23 October 2024

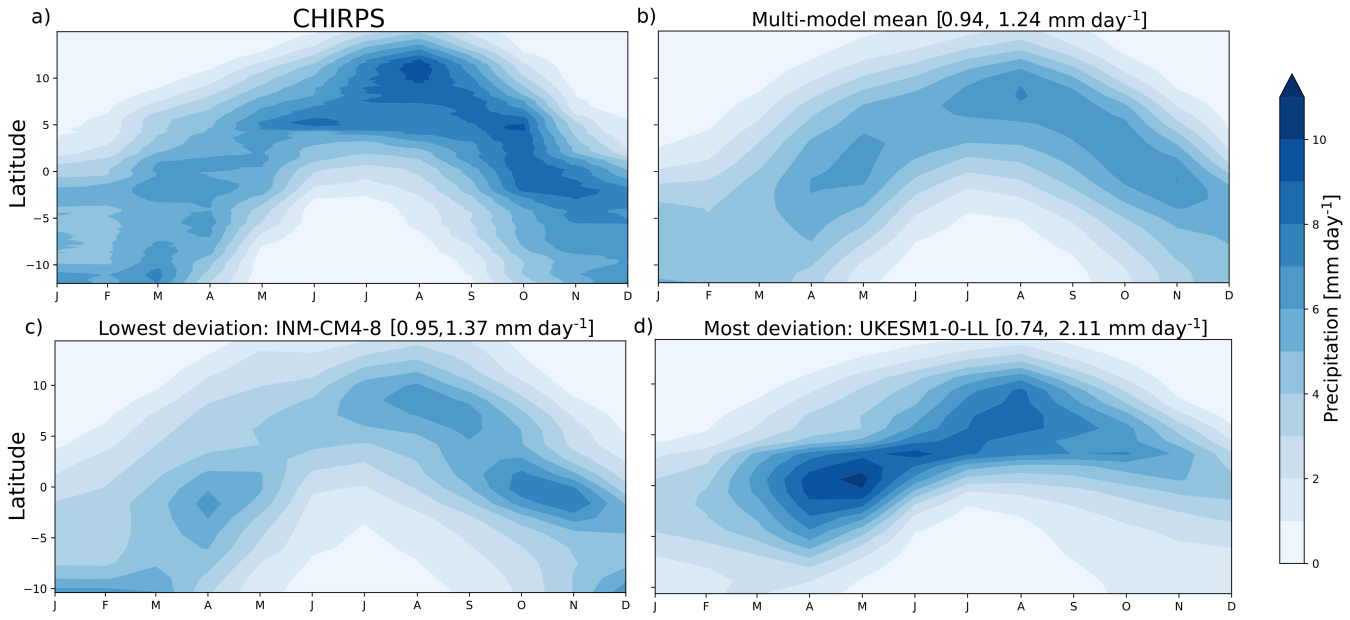

Figure 12. Latitudinal progression of the tropical rainbelt for west Africa through the seasonal cycle, averaged 1981 to 2023 for the (a) observations (CHIRPS), (b) MMM, (c) the model with the smallest deviation from observations (INM-CM4-8), (d) the model with the greatest deviation from observations (UKESM1-0-LL), with pattern correlations and RMSEs shown in square brackets above each panel. The data shown is over (10°S – 15°N, 20°W – 25°E). Units are mm day^{-1}.

in rainfall over this region in the near future is vital for informing climate adaptation. Therefore, knowledge of the biases in rainfall over this region is also needed to use CMIP6 models effectively in projections.

The latitudinal progression of the east African monsoon (EAM) throughout the year is shown in Figure 13 for observations (CHIRPS), the MMM, the model with the least deviation from CHIRPS (MIROC6), and the model with the most deviation from CHIRPS (EC-Earth3).

Model performance in capturing the progression of the EAM is slightly weaker than that of the WAM. This is reflected in the CMIP6 MMM having a pattern correlation of 0.88 (compared to 0.94 for the WAM), while individual models have patterns correlations with CHIRPS ranging from 0.91 to as low as 0.36. The EAM MMM, unlike that of the WAM, shows no strong bias in overall precipitation magnitude, and captures the northward extent of the rainband well. The evolution of rainfall is correct, though MAM (the long rains season) is too dry compared to observations, and OND (the short rains season) has a wet bias. The biases found could relate to difficulties capturing the movement of ITCZ, or impacts from the local orography being poorly represented (Munday et al., 2021, 2022).

The model with the least deviation from CHIRPS, MIROC6, is able to capture the time evolution of latitudinal progression in rainfall well. The model shows an overall wet bias common for MIROC6 over Africa — the RMSE associated with the

https://doi.org/10.5194/egusphere-2024-3057
Preprint. Discussion started: 23 October 2024

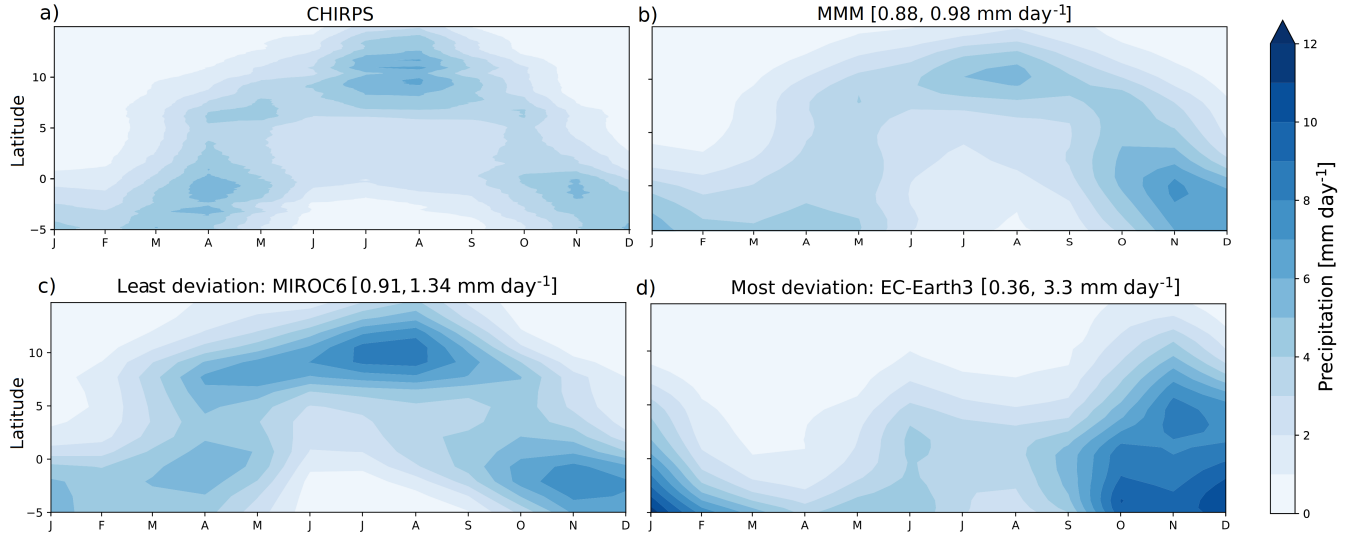

Figure 13. Latitudinal progression of the tropical rainbelt for east Africa through the seasonal cycle, averaged over 1981 to 2023 for the (a) observations (CHIRPS), (b) MMM, (c) the model with the smallest deviation from observations (MIROC6), (d) the model with the largest deviation from observations (EC-Earth3), with pattern correlations and RMSEs shown in square brackets above each panel. The data shown is over (5°S – 15°N, 27°E – 46°E). Units are mm day^{-1}.

model is higher than that of the MMM (1.34 mm day^{-1} for MIROC6, 0.98 mm day^{-1} for MMM). Overall, this model captures the latitudinal progression of rainfall over east Africa well, though the magnitude of mean rainfall is too high.

The model with the most deviation from CHIRPS, EC-Earth3, has very little resemblance to observations, with a pattern correlation of 0.36. The rainband, which in CHIRPS has a maximum intensity in MAM and OND, can be seen to only have a maximum during OND, with no other season of strong rainfall. In addition, the spatial extent 5°S–∼10°N is too large. The rainfall during this period is too strong, shown by an RMSE of 3.3 mm/day, to which the missing MAM wet season also contributes. The expected northward shift of the rainband in MAM is not present, and neither is the southward movement in SON.

Overall, the EAM is also well represented in the CMIP6 ensemble, though model performance is not as strong as for the WAM. While the absolute bias in mean precipitation is lower, the intermodel diversity is larger over this region than over West Africa, with large differences in pattern correlations and RMSEs for the models.

3.4.3 Daily precipitation

Beyond the overall temporal and spatial progression of rainfall patterns, it is important for climate models to be able to capture the characteristics of daily rainfall. As extreme events become more pronounced in a warmer world, being able to capture the extent of extreme precipitation, and the correct distribution of rainfall amounts on wet days, is integral to predicting the

https://doi.org/10.5194/egusphere-2024-3057
Preprint. Discussion started: 23 October 2024

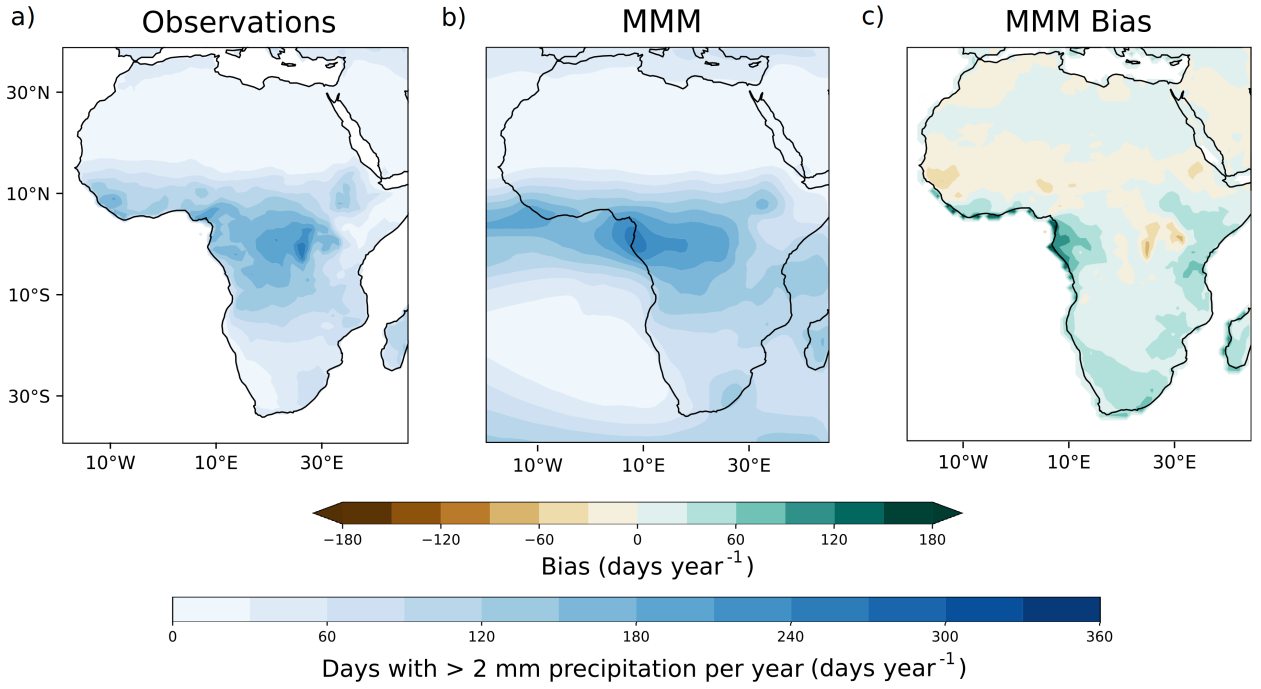

Figure 14. Number of wet days (>2 mm day^{-1}) per year for (a) CHIRPS, (b) MMM, and (c) MMM bias over Africa. The data shown is from 1981 to 2023.

changes in extremes. Africa is highly vulnerable to flooding events. This is due to many regions experiencing positive trends in both severity and frequency of flooding (Tramblay and Villarini, 2020; Ekolu et al., 2022), and there being limited resources available to these areas for flood mitigation (Di Baldassarre et al., 2010). In addition, proper daily rainfall characterization is important for the simulation of aerosol distributions and air quality (AOD and $PM_{2.5}$), as scavenging by rainfall acts to reduce aerosol lifetimes in the atmosphere. Rainfall which is too frequent, as is common in many GCMs (Emmenegger et al., 2024), is likely to lead to reduced aerosol burdens.

Figure 14 shows the number of wet days (days with > 2 mm day^{-1} rainfall) per year over Africa for observations (CHIRPS), the MMM, and the MMM bias — individual model behaviour is examined in their daily precipitation performance. This again shows a common CMIP bias, where there are too many wet days compared to observations. This bias is strongest on the west central African coast, and is substantial over this region, reaching over 160 extra wet days per year. This coincides with an area of low bias in annual mean AOD, though preliminary analysis does not show a strong relationship between increased number of wet days and decreasing AOD. The bias is also evident over areas of southern Africa and east Africa. The southward bias in rainfall is also evident through this plot. There is also a noticeable region over Uganda which has too few wet days, though the reasons for this bias over the region are not currently clear.

https://doi.org/10.5194/egusphere-2024-3057
Preprint. Discussion started: 23 October 2024

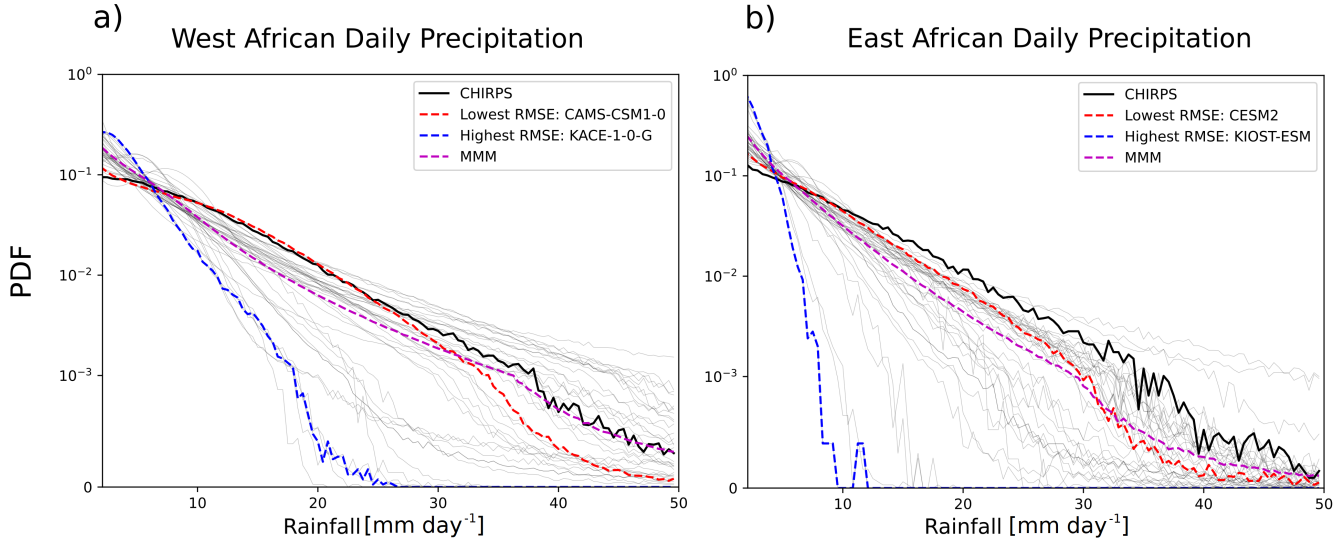

Figure 15. Probability density functions for daily rainfall on wet days (defined as >2mm day^{-1}) for each gridpoint over regions in west (a) (10°S – 15°N, 20°W – 25°E) and east (b) (5°S – 15°N, 27°E – 46°E) Africa. The multi-model mean of the distributions is shown, as well as the lowest RMSE model (CAMS-CSM1-0 for west Africa, CESM2 for east Africa), highest RMSE model (KACE-1-0-G for west Africa, KIOST-ESM for east Africa), and observations (CHIRPS). PDFs of all other models are shown in light grey lines. All models and observations have been regridded to a common 1° grid. The data shown is from 1981 to 2023.

To look more closely at daily rainfall behaviour for the monsoon regions, Figure 15 shows the probability density functions (PDFs) for daily rainfall over west and east Africa for CHIRPS, the MMM, and the models with the lowest and highest RMSEs. The PDFs are calculated from regridded daily precipitation datasets, in order to reduce the impact of differing resolutions of the different climate models and observations. Days with total rainfall of less than 2 mm are excluded from this section of analysis, to examine only the behaviour of rainfall on wet days.

As shown in Figure 15a for west Africa, the observations (CHIRPS) show a large spread of daily precipitation values, with high extremes of over 50 mm day^{-1} found in the region. In comparison, the PDFs of the MMM and highest RMSE model show that they produce too much drizzle, and the highest RMSE model fails to capture the days of very intense rainfall. This is in agreement with current literature which identifies biases with CMIP6 models producing too many days of light rainfall due to rainfall parameterisation over gridboxes (Emmenegger et al., 2024).

The model with the lowest RMSE, CAMS-CSM1-0, shows a much higher range of daily precipitation values than the MMM and highest RMSE model. CAMS-CSM1-0 captures the correct frequency of days with light rain, and only slightly underestimates the frequency of the high precipitation days.

The model with the highest RMSE, KACE-1-0-G, shows a low spread in daily precipitation values, with high frequencies associated with low daily precipitation values. In addition, the range of daily precipitation values for KACE-1-0-G extends only to 24 mm day^{-1} — less than half of the range found in CHIRPS.

https://doi.org/10.5194/egusphere-2024-3057
Preprint. Discussion started: 23 October 2024

Overall, the daily precipitation over west Africa is well represented in most models, though there are issues stemming from drizzle associated with some models, and the extreme high daily precipitation values lack representation for some models.

As shown in Figure 15b for east Africa, the observations show a slightly smaller spread in daily precipitation values, with maximum daily precipitation values of up to 50 mm day^{-1}. The shape of the PDF is similar to that of west Africa. Models over this region perform worse in replicating the behaviour of daily precipitation, especially in capturing the range of daily precipitation values.

The model with the lowest RMSE, CESM2, has a PDF showing a bias towards more days with less precipitation. Both CESM2 and the MMM fail to capture the frequency of days with intense rainfall.

The model with the highest RMSE, KIOST-ESM, has a strong bias towards days with low precipitation. The range of daily precipitation is extremely low in this model, up to 10 mm day^{-1}, showing that days of intense rainfall are not well captured by this model.

Overall, the PDF for daily precipitation is better represented over west Africa than east Africa, consistent with the representation of seasonal mean precipitation. Most models replicate the range of daily precipitation found in observations in both regions, however, a number of models produce too many days with light, but non-zero, precipitation.

4 Conclusions

We have evaluated the performance of CMIP6 models in simulating $PM_{2.5}$, AOD, and precipitation over Africa, relative to observational and reanalysis products. $PM_{2.5}$ performance, which was evaluated against a novel observational dataset, was indicated using the R^2, RMSE, and MAE metrics. For AOD and precipitation, we evaluated their performance through the use of pattern correlation coefficients and RMSEs for the seasonal mean rainfall and AOD, pattern correlation coefficients for the latitude-time progression of monsoon rainfall, and NRMSE for the seasonal cycle of AOD.

$PM_{2.5}$ concentrations derived from model mass mixing ratios are found to exhibit similar annual cycles to that of the AirNow dataset, with notable exceptions such as Cairo, though further investigation when more observational data are available for the region is necessary to reliably characterise $PM_{2.5}$ behaviour at each observation station, as current timeseries over some of the cities examined are < 1 year in length. The majority of models examined underestimate $PM_{2.5}$ concentration, which could be due to comparing observations taken in urban areas to grid cell variables, as well as the models underestimating the number of dry days identified in this analysis.

Seasonal spatial patterns of dust AOD are fairly well represented, with DJF showing the strongest disagreement with reanalysis, due to eastwards biases in the peak dust AOD from the Sahara desert, with intermodel spread cause by both interactive dust emission and circulation difference. Hotspots of intermodel disagreements over north east Africa can be linked most strongly to differences in dust emission between models. Conversely, seasonal spatial patterns of non-dust AOD are more poorly represented, with SON being the season with the strongest disagreement to reanalysis, especially in central Africa, where no models produce the area of high non-dust AOD found in CAMS, which may be due to underestimations in emissions inventories over the region. The annual cycle of AOD in CMIP6 is better represented over west Africa than east Africa, though the cycle of

https://doi.org/10.5194/egusphere-2024-3057
Preprint. Discussion started: 23 October 2024

interannual variability is not well captured for west Africa. Underestimates in emissions inventories are a potential cause of non-dust AOD biases in the MMM during SON, especially over the biomass burning regions (Reddington et al., 2016), but do not fully account for the model spread found. Difficulties in replicating the circulation over these regions are also responsible for some issues, especially model inability to correctly model transport of aerosols from biomass burning over central Africa. Further investigation of the regional biases would be possible through evaluation over smaller regions, and examination of atmospheric circulation pattern performances across Africa.

There is intermodel diversity in the position of rainfall over Africa during JJA, but the seasonal rainfall patterns are well represented for the remaining seasons. For CMIP6 models, though both are well represented, we find better performance overall in replicating the seasonal cycle of the west African monsoon than the east African monsoon. The origins for the rainfall biases over Africa may relate to biases in atmospheric circulation, such as the insufficient latitudinal progression of the ITCZ and biases in the wind bringing moisture from sea to land. Biases relating to the ITCZ appear to have a stronger effect over east Africa, where the MMM shows some biases in the timing of the rainy seasons. In contrast, difficulties with overall rainfall magnitude are more influential over west Africa, where the MMM shows a dry bias in areas impacted by the tropical rainband. Schwarzwald et al. (2022) showed that while biases in SST have some impact on precipitation performance over east Africa, changes in precipitation performance made by prescribing SSTs only improve models with difficulties in recreating features of the Indian Ocean basin, so the biases found for precipitation are unlikely to originate solely from SST biases.

The differing performances of the models based on season and region chosen underlines the need to use a diverse range of models when aiming for robust insights into the future evolution of precipitation and AOD over Africa. This study has identified model performance over Africa as a key knowledge gap, and determining the climate response to local and remote aerosol emission is crucial for Africa; these knowledge gaps are closely linked. Therefore, these findings will inform the analysis of responses found in climate projections for RAMIP experiments investigating the impacts of local and remote aerosol emission changes on Africa, modifying confidence in responses found for individual models based on their performance for the season and region of interest.

CMIP6 models exhibit large intermodel spread and biases in their simulations of air quality characteristics and precipitation patterns. When coupled with high uncertainty in future projections of African aerosol emissions, this results in a poorly constrained outlook for the future evolution of sub-Saharan air quality and precipitation. These uncertainties and disagreements with observations, alongside vulnerability to climate and air quality changes, make it challenging to accurately quantify the impacts of these changes as global warming increases and emissions of short lived climate forcers change. It is necessary to advise policy makers on emissions mitigation and local adaptation measures with clear understanding of projections and model responses. Therefore, we highlight model performance over sub-Saharan Africa and the underlying reasons for these biases as crucial knowledge gaps in atmospheric science.

Code and data availability. This work uses simulations from 56 models participating in the CMIP project as part of the Coupled Model Intercomparison Project (Phase 6; https://esgf-node.llnl.gov/search/cmip6/); model-specific information can be found through references listed

https://doi.org/10.5194/egusphere-2024-3057
Preprint. Discussion started: 23 October 2024

in Table 2. Model outputs are available on the Earth System Grid Federation (ESGF) website (https://esgf-data.dkrz.de/search/cmip6-dkrz/; Cinquini et al. (2014)). Reanalysis and observational data used in this work are all cited. The analysis was carried out using Bash and Python programming languages.

Author contributions. LJW, BHS, AGT, CAT, DMW, and JAA designed the study. JAA performed data analysis and produced the figure for $PM_{2.5}$ results and provided discussion for $PM_{2.5}$; CAT performed data analysis and produced figures for AOD and precipitation results, and discussed these results. All authors edited the paper.

Competing interests. At least one of the authors is a member of the editorial board of *Atmospheric Chemistry and Physics*.

Acknowledgements. LJW and AGT are supported by the Natural Environment Research Council (NERC; grant NE/W004895/1, TerraFIRMA) and the National Centre for Atmospheric Science. We acknowledge the Centre for Advanced Study in Oslo, Norway, which funded and hosted our HETCLIF centre during the academic year of 2023/2024. DMW and JAA are supported by US National Science Foundation Office of International Science and Engineering Grant 2020677. BHS acknowledges funding from the Research Council of Norway, Grant 324182 (CATHY). CAT acknowledges PhD studentship funding from SCENARIO Natural Environment Research Council (NERC) Doctoral Training Partnership grant and a CICERO CASE studentship. We acknowledge the World Climate Research Programme, which, through its Working Group on Coupled Modelling, coordinated and promoted CMIP6. We thank the climate modelling groups for producing and making available their model output, the Earth System Grid Federation (ESGF) for archiving the data and providing access, and the multiple funding agencies who support CMIP6 and ESGF. We acknowledge the use of ERA5 data produced by ECMWF, CHIRPS data produced by the Climate Hazards Center, and CAMS data produced by ECMWF. Additional details of ERA5 and CAMS can be found at https://cds.climate.copernicus.eu/ (last access: 26 September 2024), CHIRPS at https://www.chc.ucsb.edu/data/chirps (last access: 30 September 2024), or CAMS at . The analysis in this work was performed on the JASMIN super-data cluster (Lawrence et al., 2012). JASMIN is managed and delivered by the UK Science and Technology Facilities Council (STFC) Centre for Environmental Data Analysis (CEDA).

https://doi.org/10.5194/egusphere-2024-3057
Preprint. Discussion started: 23 October 2024

References

AERONET: Aerosol Robotic Network (AERONET) Homepage — aeronet.gsfc.nasa.gov, https://aeronet.gsfc.nasa.gov, [Accessed 29-03-2024], 2024.

AirNow: US Embassies and Consulates | AirNow.gov — airnow.gov, https://www.airnow.gov/international/us-embassies-and-consulates/, [Accessed 29-03-2024], 2021.

Andrews, M. B., Ridley, J. K., Wood, R. A., Andrews, T., Blockley, E. W., Booth, B., Burke, E., Dittus, A. J., Florek, P., Gray, L. J., Haddad, S., Hardiman, S. C., Hermanson, L., Hodson, D., Hogan, E., Jones, G. S., Knight, J. R., Kuhlbrodt, T., Misios, S., Mizielinski, M. S., Ringer, M. A., Robson, J., and Sutton, R. T.: Historical Simulations With HadGEM3-GC3.1 for CMIP6, Journal of Advances in Modeling Earth Systems, 12, e2019MS001 995, https://doi.org/https://doi.org/10.1029/2019MS001995, e2019MS001995 10.1029/2019MS001995, 2020.

Annor, T., Ackon, A. T., James, R., Dyer, E., Webb, T., Pokam, W. M., Kuete Gouandjo, G., Washington, R., and Abiodun, B. J.: Heat band, rain band and heat low migration: process-based evaluation of some CMIP6 GCMs over West Africa, Clim. Dyn., 2023.

Anuforom, A. C.: Spatial distribution and temporal variability of Harmattan dust haze in sub-Sahel West Africa, Atmos. Environ. (1994), 41, 9079–9090, 2007.

Archer-Nicholls, S., Allen, R., Abraham, N. L., Griffiths, P. T., and Archibald, A. T.: Large simulated future changes in the nitrate radical under the CMIP6 SSP scenarios: implications for oxidation chemistry, Atmos. Chem. Phys., 23, 5801–5813, 2023.

Ayehu, G. T., Tadesse, T., Gessesse, B., and Dinku, T.: Validation of new satellite rainfall products over the Upper Blue Nile Basin, Ethiopia, Atmospheric Measurement Techniques, 11, 1921–1936, https://doi.org/10.5194/amt-11-1921-2018, 2018.

Ayugi, B., Zhihong, J., Zhu, H., Ngoma, H., Babaousmail, H., Rizwan, K., and Dike, V.: Comparison of CMIP6 and CMIP5 models in simulating mean and extreme precipitation over East Africa, Int. J. Climatol., 41, 6474–6496, 2021.

Ayugi, B. O., Chung, E.-S., Babaousmail, H., and Lim Kam Sian, K. T. C.: Characterizing the performances of different observational precipitation products and their uncertainties over Africa, Environ. Res. Lett., 19, 064 009, 2024.

Bader, D. C., Leung, R., Taylor, M., and McCoy, R. B.: E3SM-Project E3SM1.0 model output prepared for CMIP6 CMIP historical, https://doi.org/10.22033/ESGF/CMIP6.4497, 2019a.

Bader, D. C., Leung, R., Taylor, M., and McCoy, R. B.: E3SM-Project E3SM1.1 model output prepared for CMIP6 CMIP historical, https://doi.org/10.22033/ESGF/CMIP6.11485, 2019b.

Bader, D. C., Leung, R., Taylor, M., and McCoy, R. B.: E3SM-Project E3SM1.1ECA model output prepared for CMIP6 CMIP historical, 2020.

Bader, D. C., Leung, R., Taylor, M., and McCoy, R. B.: E3SM-Project E3SM2.0NARRM model output prepared for CMIP6 CMIP amip, 2023.

Bauer, S. E., Im, U., Mezuman, K., and Gao, C. Y.: Desert dust, industrialization and agricultural fires: Health impacts of outdoor air pollution in Africa, Journal of Geophysical Research: Atmospheres, 124, 4104–4120, https://doi.org/10.1029/2018JD029336, 2019.

Beck, H. E., Vergopolan, N., Pan, M., Levizzani, V., van Dijk, A. I. J. M., Weedon, G. P., Brocca, L., Pappenberger, F., Huffman, G. J., and Wood, E. F.: Global-scale evaluation of 22 precipitation datasets using gauge observations and hydrological modeling, Hydrol. Earth Syst. Sci., 21, 6201–6217, 2017.

Bentsen, M., Oliviè, D. J. L., Seland, y., Toniazzo, T., Gjermundsen, A., Graff, L. S., Debernard, J. B., Gupta, A. K., He, Y., Kirkevåg, A., Schwinger, J., Tjiputra, J., Aas, K. S., Bethke, I., Fan, Y., Griesfeller, J., Grini, A., Guo, C., Ilicak, M., Karset, I. H. H., Landgren,

https://doi.org/10.5194/egusphere-2024-3057
Preprint. Discussion started: 23 October 2024

O. A., Liakka, J., Moseid, K. O., Nummelin, A., Spensberger, C., Tang, H., Zhang, Z., Heinze, C., Iversen, T., and Schulz, M.: NCC NorESM2-MM model output prepared for CMIP6 CMIP historical, https://doi.org/10.22033/ESGF/CMIP6.8040, 2019.

Bethke, I., Wang, Y., Counillon, F., Kimmritz, M., Fransner, F., Samuelsen, A., Langehaug, H. R., Chiu, P.-G., Bentsen, M., Guo, C., Tjiputra, J., Kirkevåg, A., Oliviè, D. J. L., Seland, y., Fan, Y., Lawrence, P., Eldevik, T., and Keenlyside, N.: NCC NorCPM1 model output prepared for CMIP6 CMIP historical, https://doi.org/10.22033/ESGF/CMIP6.10894, 2019.

Bock, L., Lauer, A., Schlund, M., Barreiro, M., Bellouin, N., Jones, C., Meehl, G. A., Predoi, V., Roberts, M. J., and Eyring, V.: Quantifying Progress Across Different CMIP Phases With the ESMValTool, Journal of Geophysical Research: Atmospheres, 125, https://doi.org/10.1029/2019jd032321, 2020.

Booyens, W., Beukes, J. P., Van Zyl, P. G., Ruiz-Jimenez, J., Kopperi, M., Riekkola, M.-L., Josipovic, M., Vakkari, V., and Laakso, L.: Summary of research paper published in Journal of Atmospheric Chemistry titled: Assessment of polar organic aerosols at a regional background site in southern Africa, Clean Air Journal, 29, https://doi.org/10.17159/2410-972x/2019/v29n1a10, 2019.

Boucher, O., Randall, D., Artaxo, P., Bretherton, C., Feingold, G., Forster, P., Kerminen, V.-M., Kondo, Y., Liao, H., Lohmann, U., et al.: Clouds and aerosols, in: Climate change 2013: the physical science basis. Contribution of Working Group I to the Fifth Assessment Report of the Intergovernmental Panel on Climate Change, pp. 571–657, Cambridge University Press, https://doi.org/10.1017/CBO9781107415324.016, 2013.

Boucher, O., Denvil, S., Levavasseur, G., Cozic, A., Caubel, A., Foujols, M.-A., Meurdesoif, Y., Cadule, P., Devilliers, M., Dupont, E., and Lurton, T.: IPSL IPSL-CM5A2-INCA model output prepared for CMIP6 ScenarioMIP ssp370, 2020a.

Boucher, O., Servonnat, J., Albright, A. L., Aumont, O., Balkanski, Y., Bastrikov, V., Bekki, S., Bonnet, R., Bony, S., Bopp, L., Braconnot, P., Brockmann, P., Cadule, P., Caubel, A., Cheruy, F., Codron, F., Cozic, A., Cugnet, D., D'Andrea, F., Davini, P., de Lavergne, C., Denvil, S., Deshayes, J., Devilliers, M., Ducharne, A., Dufresne, J.-L., Dupont, E., Éthé, C., Fairhead, L., Falletti, L., Flavoni, S., Foujols, M.-A., Gardoll, S., Gastineau, G., Ghattas, J., Grandpeix, J.-Y., Guenet, B., Guez, Lionel, E., Guilyardi, E., Guimberteau, M., Hauglustaine, D., Hourdin, F., Idelkadi, A., Joussaume, S., Kageyama, M., Khodri, M., Krinner, G., Lebas, N., Levavasseur, G., Lévy, C., Li, L., Lott, F., Lurton, T., Luyssaert, S., Madec, G., Madeleine, J.-B., Maignan, F., Marchand, M., Marti, O., Mellul, L., Meurdesoif, Y., Mignot, J., Musat, I., Ottlé, C., Peylin, P., Planton, Y., Polcher, J., Rio, C., Rochetin, N., Rousset, C., Sepulchre, P., Sima, A., Swingedouw, D., Thiéblemont, R., Traore, A. K., Vancoppenolle, M., Vial, J., Vialard, J., Viovy, N., and Vuichard, N.: Presentation and Evaluation of the IPSL-CM6A-LR Climate Model, Journal of Advances in Modeling Earth Systems, 12, e2019MS002 010, https://doi.org/https://doi.org/10.1029/2019MS002010, e2019MS002010 10.1029/2019MS002010, 2020b.

Boucher, O., Denvil, S., Levavasseur, G., Cozic, A., Caubel, A., Foujols, M.-A., Meurdesoif, Y., Balkanski, Y., Checa-Garcia, R., Hauglustaine, D., Bekki, S., and Marchand, M.: IPSL IPSL-CM6A-LR-INCA model output prepared for CMIP6 CMIP historical, 2021a.

Boucher, O., Denvil, S., Levavasseur, G., Cozic, A., Caubel, A., Foujols, M.-A., Meurdesoif, Y., Balkanski, Y., Checa-Garcia, R., Hauglustaine, D., Bekki, S., and Marchand, M.: IPSL IPSL-CM6A-LR-INCA model output prepared for CMIP6 CMIP historical, https://doi.org/10.22033/ESGF/CMIP6.13601, 2021b.

Burrows, S. M., Maltrud, M., Yang, X., Zhu, Q., Jeffery, N., Shi, X., Ricciuto, D., Wang, S., Bisht, G., Tang, J., Wolfe, J., Harrop, B. E., Singh, B., Brent, L., Baldwin, S., Zhou, T., Cameron-Smith, P., Keen, N., Collier, N., Xu, M., Hunke, E. C., Elliott, S. M., Turner, A. K., Li, H., Wang, H., Golaz, J.-C., Bond-Lamberty, B., Hoffman, F. M., Riley, W. J., Thornton, P. E., Calvin, K., and Leung, L. R.: The DOE E3SM v1.1 biogeochemistry configuration: Description and simulated ecosystem-climate responses to historical changes in forcing, J. Adv. Model. Earth Syst., 12, 2020.

https://doi.org/10.5194/egusphere-2024-3057
Preprint. Discussion started: 23 October 2024

Byun, Y.-H., Lim, Y.-J., Sung, H. M., Kim, J., Sun, M., and Kim, B.-H.: NIMS-KMA KACE1.0-G model output prepared for CMIP6 CMIP historical, https://doi.org/10.22033/ESGF/CMIP6.8378, 2019.

Chen, D., Rojas, M., Samset, B., Cobb, K., Diongue Niang, A., Edwards, P., Emori, S., Faria, S., Hawkins, E., Hope, P., Huybrechts, P., Meinshausen, M., Mustafa, S., Plattner, G.-K., and Tréguier, A.-M.: Framing, Context, and Methods, p. 147–286, Cambridge University Press, Cambridge, United Kingdom and New York, NY, USA, https://doi.org/10.1017/9781009157896.003, 2021.

Cherchi, A., Fogli, P. G., Lovato, T., Peano, D., Iovino, D., Gualdi, S., Masina, S., Scoccimarro, E., Materia, S., Bellucci, A., and Navarra, A.: Global Mean Climate and Main Patterns of Variability in the CMCC-CM2 Coupled Model, Journal of Advances in Modeling Earth Systems, 11, 185–209, https://doi.org/https://doi.org/10.1029/2018MS001369, 2019.

Christian, J. R., Denman, K. L., Hayashida, H., Holdsworth, A. M., Lee, W. G., Riche, O. G. J., Shao, A. E., Steiner, N., and Swart, N. C.: Ocean biogeochemistry in the Canadian Earth System Model version 5.0.3: CanESM5 and CanESM5-CanOE, Geoscientific Model Development, 15, 4393–4424, https://doi.org/10.5194/gmd-15-4393-2022, 2022.

Cinquini, L., Crichton, D., Mattmann, C., Harney, J., Shipman, G., Wang, F., Ananthakrishnan, R., Miller, N., Denvil, S., Morgan, M., Pobre, Z., Bell, G. M., Doutriaux, C., Drach, R., Williams, D., Kershaw, P., Pascoe, S., Gonzalez, E., Fiore, S., and Schweitzer, R.: The Earth System Grid Federation: An open infrastructure for access to distributed geospatial data, Future Generation Computer Systems, 36, 400–417, https://doi.org/10.1016/j.future.2013.07.002, 2014.

Cook, K. H.: Generation of the African Easterly Jet and Its Role in Determining West African Precipitation, Journal of Climate, 12, 1165–1184, https://doi.org/10.1175/1520-0442(1999)012<1165:GOTAEJ>2.0.CO;2, 1999.

Copans, J.: The Sahelian drought: social sciences and the political economy of underdevelopment, pp. 83–97, ISBN 9780429329579, https://doi.org/10.4324/9780429329579-5, 2019.

Danabasoglu, G.: NCAR CESM2-FV2 model output prepared for CMIP6 CMIP historical, https://doi.org/10.22033/ESGF/CMIP6.11297, 2019a.

Danabasoglu, G.: NCAR CESM2-WACCM model output prepared for CMIP6 CMIP historical, https://doi.org/10.22033/ESGF/CMIP6.10071, 2019b.

Danabasoglu, G.: NCAR CESM2 model output prepared for CMIP6 CMIP historical, https://doi.org/10.22033/ESGF/CMIP6.7627, 2019c.

Danabasoglu, G., Lamarque, J.-F., Bacmeister, J., Bailey, D. A., DuVivier, A. K., Edwards, J., Emmons, L. K., Fasullo, J., Garcia, R., Gettelman, A., Hannay, C., Holland, M. M., Large, W. G., Lauritzen, P. H., Lawrence, D. M., Lenaerts, J. T. M., Lindsay, K., Lipscomb, W. H., Mills, M. J., Neale, R., Oleson, K. W., Otto-Bliesner, B., Phillips, A. S., Sacks, W., Tilmes, S., van Kampenhout, L., Vertenstein, M., Bertini, A., Dennis, J., Deser, C., Fischer, C., Fox-Kemper, B., Kay, J. E., Kinnison, D., Kushner, P. J., Larson, V. E., Long, M. C., Mickelson, S., Moore, J. K., Nienhouse, E., Polvani, L., Rasch, P. J., and Strand, W. G.: The Community Earth System Model Version 2 (CESM2), Journal of Advances in Modeling Earth Systems, 12, e2019MS001 916, https://doi.org/https://doi.org/10.1029/2019MS001916, e2019MS001916 2019MS001916, 2020.

Danek, C., Shi, X., Stepanek, C., Yang, H., Barbi, D., Hegewald, J., and Lohmann, G.: AWI AWI-ESM1.1LR model output prepared for CMIP6 CMIP historical, https://doi.org/10.22033/ESGF/CMIP6.9328, 2020.

Di Baldassarre, G., Montanari, A., Lins, H., Koutsoyiannis, D., Brandimarte, L., and Blöschl, G.: Flood fatalities in Africa: From diagnosis to mitigation, Geophysical Research Letters, 37, https://doi.org/10.1029/2010gl045467, 2010.

Diem, J. E., Sung, H. S., Konecky, B. L., Palace, M. W., Salerno, J., and Hartter, J.: Rainfall Characteristics and Trends—and the Role of Congo Westerlies—in the Western Uganda Transition Zone of Equatorial Africa From 1983 to 2017, Journal of Geophysical Research: Atmospheres, 124, 10 712–10 729, https://doi.org/10.1029/2019jd031243, 2019.

https://doi.org/10.5194/egusphere-2024-3057
Preprint. Discussion started: 23 October 2024

Dinku, T., Funk, C., Peterson, P., Maidment, R., Tadesse, T., Gadain, H., and Ceccato, P.: Validation of the CHIRPS satellite rainfall estimates over eastern Africa, Quarterly Journal of the Royal Meteorological Society, 144, 292–312, https://doi.org/10.1002/qj.3244, 2018.

Dix, M., Bi, D., Dobrohotoff, P., Fiedler, R., Harman, I., Law, R., Mackallah, C., Marsland, S., O'Farrell, S., Rashid, H., Srbinovsky, J., Sullivan, A., Trenham, C., Vohralik, P., Watterson, I., Williams, G., Woodhouse, M., Bodman, R., Dias, F. B., Domingues, C., Hannah, N., Heerdegen, A., Savita, A., Wales, S., Allen, C., Druken, K., Evans, B., Richards, C., Ridzwan, S. M., Roberts, D., Smillie, J., Snow, K., Ward, M., and Yang, R.: CSIRO-ARCCSS ACCESS-CM2 model output prepared for CMIP6 CMIP historical, https://doi.org/10.22033/ESGF/CMIP6.4271, 2019.

Dixon, R. D., Daloz, A. S., Vimont, D. J., and Biasutti, M.: Saharan Heat Low Biases in CMIP5 Models, Journal of Climate, 30, 2867–2884, https://doi.org/10.1175/JCLI-D-16-0134.1, 2017.

Dong, B., Sutton, R. T., Highwood, E., and Wilcox, L.: The Impacts of European and Asian Anthropogenic Sulfur Dioxide Emissions on Sahel Rainfall, Journal of Climate, 27, 7000–7017, https://doi.org/10.1175/jcli-d-13-00769.1, 2014.

Dunne, J. P., Horowitz, L. W., Adcroft, A. J., Ginoux, P., Held, I. M., John, J. G., Krasting, J. P., Malyshev, S., Naik, V., Paulot, F., Shevliakova, E., Stock, C. A., Zadeh, N., Balaji, V., Blanton, C., Dunne, K. A., Dupuis, C., Durachta, J., Dussin, R., Gauthier, P. P. G., Griffies, S. M., Guo, H., Hallberg, R. W., Harrison, M., He, J., Hurlin, W., McHugh, C., Menzel, R., Milly, P. C. D., Nikonov, S., Paynter, D. J., Ploshay, J., Radhakrishnan, A., Rand, K., Reichl, B. G., Robinson, T., Schwarzkopf, D. M., Sentman, L. T., Underwood, S., Vahlenkamp, H., Winton, M., Wittenberg, A. T., Wyman, B., Zeng, Y., and Zhao, M.: The GFDL Earth System Model Version 4.1 (GFDL-ESM 4.1): Overall Coupled Model Description and Simulation Characteristics, Journal of Advances in Modeling Earth Systems, 12, e2019MS002 015, https://doi.org/https://doi.org/10.1029/2019MS002015, e2019MS002015 2019MS002015, 2020.

Ekolu, J., Dieppois, B., Sidibe, M., Eden, J. M., Tramblay, Y., Villarini, G., Peña-Angulo, D., Mahé, G., Paturel, J.-E., Onyutha, C., and van de Wiel, M.: Long-term variability in hydrological droughts and floods in sub-Saharan Africa: New perspectives from a 65-year daily streamflow dataset, Journal of Hydrology, 613, 128 359, https://doi.org/10.1016/j.jhydrol.2022.128359, 2022.

Emmenegger, T., Ahmed, F., Kuo, Y.-H., Xie, S., Zhang, C., Tao, C., and Neelin, J. D.: The physics behind precipitation onset bias in CMIP6 models: The pseudo-entrainment diagnostic and trade-offs between lapse rate and humidity, J. Clim., 37, 2013–2033, 2024.

Eyring, V., Bony, S., Meehl, G. A., Senior, C. A., Stevens, B., Stouffer, R. J., and Taylor, K. E.: Overview of the Coupled Model Intercomparison Project Phase 6 (CMIP6) experimental design and organization, Geosci. Model Dev., 9, 1937–1958, 2016.

Fiedler, S., van Noije, T., Smith, C. J., Boucher, O., Dufresne, J.-L., Kirkevåg, A., Olivié, D., Pinto, R., Reerink, T., Sima, A., and Schulz, M.: Historical changes and reasons for model differences in anthropogenic aerosol forcing in CMIP6, Geophys. Res. Lett., 50, 2023.

Fosu-Amankwah, K., Bessardon, G. E., Quansah, E., Amekudzi, L. K., Brooks, B. J., and Damoah, R.: Assessment of aerosol burden over Ghana, Scientific African, 14, e00 971, https://doi.org/10.1016/j.sciaf.2021.e00971, 2021.

Funk, C., Peterson, P., Landsfeld, M., Pedreros, D., Verdin, J., Shukla, S., Husak, G., Rowland, J., Harrison, L., Hoell, A., and Michaelsen, J.: The climate hazards infrared precipitation with stations—a new environmental record for monitoring extremes, Scientific Data, 2, https://doi.org/10.1038/sdata.2015.66, 2015.

Fuzzi, S., Baltensperger, U., Carslaw, K., Decesari, S., Denier van der Gon, H., Facchini, M. C., Fowler, D., Koren, I., Langford, B., Lohmann, U., Nemitz, E., Pandis, S., Riipinen, I., Rudich, Y., Schaap, M., Slowik, J. G., Spracklen, D. V., Vignati, E., Wild, M., Williams, M., and Gilardoni, S.: Particulate matter, air quality and climate: lessons learned and future needs, Atmospheric Chemistry and Physics, 15, 8217–8299, https://doi.org/10.5194/acp-15-8217-2015, 2015.

Garrigues, S., Remy, S., Chimot, J., Ades, M., Inness, A., Flemming, J., Kipling, Z., Laszlo, I., Benedetti, A., Ribas, R., Jafariserajehlou, S., Fougnie, B., Kondragunta, S., Engelen, R., Peuch, V.-H., Parrington, M., Bousserez, N., Vazquez Navarro, M., and Agusti-Panareda, A.:

https://doi.org/10.5194/egusphere-2024-3057
Preprint. Discussion started: 23 October 2024

Monitoring multiple satellite aerosol optical depth (AOD) products within the Copernicus Atmosphere Monitoring Service (CAMS) data assimilation system, Atmos. Chem. Phys., 22, 14 657–14 692, 2022.

Gidden, M., Riahi, K., Smith, S., Fujimori, S., Luderer, G., Kriegler, E., van Vuuren, D., van den Berg, M., Feng, L., Klein, D., Calvin, K., Doelman, J., Frank, S., Fricko, O., Harmsen, M., Hasegawa, T., Havlik, P., Hilaire, J., Hoesly, R., Horing, J., Popp, A., Stehfest, E., and Takahashi, K.: input4MIPs.CMIP6.ScenarioMIP.IAMC, https://doi.org/10.22033/ESGF/INPUT4MIPS.10464, 2018.

GISS, N.: NASA-GISS GISS-E2.1G model output prepared for CMIP6 CMIP historical, https://doi.org/10.22033/ESGF/CMIP6.7127, 2018.

GISS, N.: NASA-GISS GISS-E2-1-G-CC model output prepared for CMIP6 CMIP historical, https://doi.org/10.22033/ESGF/CMIP6.11762, 2019a.

GISS, N.: NASA-GISS GISS-E2.1H model output prepared for CMIP6 CMIP historical, https://doi.org/10.22033/ESGF/CMIP6.7128, 2019b.

Glantz, M. H., ed.: Politics of natural disaster, Praeger special studies in international economics and development, Praeger, Westport, CT, 1976.

Golaz, J.-C., Caldwell, P. M., Van Roekel, L. P., Petersen, M. R., Tang, Q., Wolfe, J. D., Abeshu, G., Anantharaj, V., Asay-Davis, X. S., Bader, D. C., Baldwin, S. A., Bisht, G., Bogenschutz, P. A., Branstetter, M., Brunke, M. A., Brus, S. R., Burrows, S. M., Cameron-Smith, P. J., Donahue, A. S., Deakin, M., Easter, R. C., Evans, K. J., Feng, Y., Flanner, M., Foucar, J. G., Fyke, J. G., Griffin, B. M., Hannay, C., Harrop, B. E., Hoffman, M. J., Hunke, E. C., Jacob, R. L., Jacobsen, D. W., Jeffery, N., Jones, P. W., Keen, N. D., Klein, S. A., Larson, V. E., Leung, L. R., Li, H.-Y., Lin, W., Lipscomb, W. H., Ma, P.-L., Mahajan, S., Maltrud, M. E., Mametjanov, A., McClean, J. L., McCoy, R. B., Neale, R. B., Price, S. F., Qian, Y., Rasch, P. J., Reeves Eyre, J. E. J., Riley, W. J., Ringler, T. D., Roberts, A. F., Roesler, E. L., Salinger, A. G., Shaheen, Z., Shi, X., Singh, B., Tang, J., Taylor, M. A., Thornton, P. E., Turner, A. K., Veneziani, M., Wan, H., Wang, H., Wang, S., Williams, D. N., Wolfram, P. J., Worley, P. H., Xie, S., Yang, Y., Yoon, J.-H., Zelinka, M. D., Zender, C. S., Zeng, X., Zhang, C., Zhang, K., Zhang, Y., Zheng, X., Zhou, T., and Zhu, Q.: The DOE E3SM Coupled Model Version 1: Overview and Evaluation at Standard Resolution, Journal of Advances in Modeling Earth Systems, 11, 2089–2129, https://doi.org/https://doi.org/10.1029/2018MS001603, 2019.

Golaz, J.-C., Van Roekel, L. P., Zheng, X., Roberts, A. F., Wolfe, J. D., Lin, W., Bradley, A. M., Tang, Q., Maltrud, M. E., Forsyth, R. M., Zhang, C., Zhou, T., Zhang, K., Zender, C. S., Wu, M., Wang, H., Turner, A. K., Singh, B., Richter, J. H., Qin, Y., Petersen, M. R., Mametjanov, A., Ma, P.-L., Larson, V. E., Krishna, J., Keen, N. D., Jeffery, N., Hunke, E. C., Hannah, W. M., Guba, O., Griffin, B. M., Feng, Y., Engwirda, D., Di Vittorio, A. V., Dang, C., Conlon, L. M., Chen, C.-C.-J., Brunke, M. A., Bisht, G., Benedict, J. J., Asay-Davis, X. S., Zhang, Y., Zhang, M., Zeng, X., Xie, S., Wolfram, P. J., Vo, T., Veneziani, M., Tesfa, T. K., Sreepathi, S., Salinger, A. G., Reeves Eyre, J. E. J., Prather, M. J., Mahajan, S., Li, Q., Jones, P. W., Jacob, R. L., Huebler, G. W., Huang, X., Hillman, B. R., Harrop, B. E., Foucar, J. G., Fang, Y., Comeau, D. S., Caldwell, P. M., Bartoletti, T., Balaguru, K., Taylor, M. A., McCoy, R. B., Leung, L. R., and Bader, D. C.: The DOE E3SM model version 2: Overview of the physical model and initial model evaluation, J. Adv. Model. Earth Syst., 14, 2022.

Guo, H., John, J. G., Blanton, C., McHugh, C., Nikonov, S., Radhakrishnan, A., Rand, K., Zadeh, N. T., Balaji, V., Durachta, J., Dupuis, C., Menzel, R., Robinson, T., Underwood, S., Vahlenkamp, H., Bushuk, M., Dunne, K. A., Dussin, R., Gauthier, P. P., Ginoux, P., Griffies, S. M., Hallberg, R., Harrison, M., Hurlin, W., Lin, P., Malyshev, S., Naik, V., Paulot, F., Paynter, D. J., Ploshay, J., Reichl, B. G., Schwarzkopf, D. M., Seman, C. J., Shao, A., Silvers, L., Wyman, B., Yan, X., Zeng, Y., Adcroft, A., Dunne, J. P., Held, I. M., Krasting, J. P., Horowitz, L. W., Milly, P., Shevliakova, E., Winton, M., Zhao, M., and Zhang, R.: NOAA-GFDL GFDL-CM4 model output historical, https://doi.org/10.22033/ESGF/CMIP6.8594, 2018.

https://doi.org/10.5194/egusphere-2024-3057
Preprint. Discussion started: 23 October 2024

Gupta, A. K., Deshmukh, A., Waman, D., Patade, S., Jadav, A., Phillips, V. T. J., Bansemer, A., Martins, J. A., and Gonçalves, F. L. T.: The microphysics of the warm-rain and ice crystal processes of precipitation in simulated continental convective storms, Communications Earth & Environment, 4, https://doi.org/10.1038/s43247-023-00884-5, 2023.

Hagler, G., Hanley, T., Hassett-Sipple, B., Vanderpool, R., Smith, M., Wilbur, J., Wilbur, T., Oliver, T., Shand, D., Vidacek, V., Johnson, C., Allen, R., and D'Angelo, C.: Evaluation of two collocated federal equivalent method PM2.5 instruments over a wide range of concentrations in Sarajevo, Bosnia and Herzegovina, Atmospheric Pollution Research, 13, 101 374, https://doi.org/10.1016/j.apr.2022.101374, 2022.

Hajima, T., Abe, M., Arakawa, O., Suzuki, T., Komuro, Y., Ogura, T., Ogochi, K., Watanabe, M., Yamamoto, A., Tatebe, H., Noguchi, M. A., Ohgaito, R., Ito, A., Yamazaki, D., Ito, A., Takata, K., Watanabe, S., Kawamiya, M., and Tachiiri, K.: MIROC MIROC-ES2L model output prepared for CMIP6 CMIP historical, https://doi.org/10.22033/ESGF/CMIP6.5602, 2019.

Hajima, T., Watanabe, M., Yamamoto, A., Tatebe, H., Noguchi, M. A., Abe, M., Ohgaito, R., Ito, A., Yamazaki, D., Okajima, H., Ito, A., Takata, K., Ogochi, K., Watanabe, S., and Kawamiya, M.: Development of the MIROC-ES2L Earth system model and the evaluation of biogeochemical processes and feedbacks, Geoscientific Model Development, 13, 2197–2244, https://doi.org/10.5194/gmd-13-2197-2020, 2020.

Hao-Ming CHEN, Jian LI, J.-Z. S. L.-J. H. X.-Y. R. Y.-F. X. Z.-Q. Z.: Introduction of CAMS-CSM model and its participation in CMIP6, Advances in Climate Change Research, 15, 540–544, 2019.

Hastenrath, S., Polzin, D., and Mutai, C.: Circulation Mechanisms of Kenya Rainfall Anomalies, Journal of Climate, 24, 404–412, https://doi.org/10.1175/2010jcli3599.1, 2011.

He, B., Yu, Y., Bao, Q., Lin, P., Liu, H., Li, J., Wang, L., Liu, Y., Wu, G., Chen, K., Guo, Y., Zhao, S., Zhang, X., Song, M., and Xie, J.: CAS FGOALS-f3-L model dataset descriptions for CMIP6 DECK experiments, Atmospheric and Oceanic Science Letters, 13, 582–588, https://doi.org/10.1080/16742834.2020.1778419, 2020.

Health Effects Institute: The State of Air Quality and Health Impacts in Africa | State of Global Air — stateofglobalair.org, https://www.stateofglobalair.org/resources/report/state-air-quality-and-health-impacts-africa, [Accessed 28-03-2024], 2022.

Held, I. M., Guo, H., Adcroft, A., Dunne, J. P., Horowitz, L. W., Krasting, J., Shevliakova, E., Winton, M., Zhao, M., Bushuk, M., Wittenberg, A. T., Wyman, B., Xiang, B., Zhang, R., Anderson, W., Balaji, V., Donner, L., Dunne, K., Durachta, J., Gauthier, P. P. G., Ginoux, P., Golaz, J.-C., Griffies, S. M., Hallberg, R., Harris, L., Harrison, M., Hurlin, W., John, J., Lin, P., Lin, S.-J., Malyshev, S., Menzel, R., Milly, P. C. D., Ming, Y., Naik, V., Paynter, D., Paulot, F., Rammaswamy, V., Reichl, B., Robinson, T., Rosati, A., Seman, C., Silvers, L. G., Underwood, S., and Zadeh, N.: Structure and Performance of GFDL's CM4.0 Climate Model, Journal of Advances in Modeling Earth Systems, 11, 3691–3727, https://doi.org/https://doi.org/10.1029/2019MS001829, 2019.

Hersbach, H., Bell, B., Berrisford, P., Hirahara, S., Horányi, A., Muñoz-Sabater, J., Nicolas, J., Peubey, C., Radu, R., Schepers, D., Simmons, A., Soci, C., Abdalla, S., Abellan, X., Balsamo, G., Bechtold, P., Biavati, G., Bidlot, J., Bonavita, M., De Chiara, G., Dahlgren, P., Dee, D., Diamantakis, M., Dragani, R., Flemming, J., Forbes, R., Fuentes, M., Geer, A., Haimberger, L., Healy, S., Hogan, R. J., Hólm, E., Janisková, M., Keeley, S., Laloyaux, P., Lopez, P., Lupu, C., Radnoti, G., de Rosnay, P., Rozum, I., Vamborg, F., Villaume, S., and Jean-Noël Thépaut: The ERA5 global reanalysis, Q. J. R. Meteorol. Soc., 146, 1999–2049, 2020.

Huang, W.: THU CIESM model output prepared for CMIP6 CMIP historical, https://doi.org/10.22033/ESGF/CMIP6.8843, 2019.

Huffman, G. J., Adler, R. F., Behrangi, A., Bolvin, D. T., Nelkin, E. J., Gu, G., and Ehsani, M. R.: The new Version 3.2 Global Precipitation Climatology Project (GPCP) monthly and daily precipitation products, J. Clim., 36, 7635–7655, 2023.

https://doi.org/10.5194/egusphere-2024-3057
Preprint. Discussion started: 23 October 2024

Hulme, M.: Climatic perspectives on Sahelian desiccation: 1973–1998, Global Environmental Change, 11, 19–29, https://doi.org/10.1016/s0959-3780(00)00042-x, 2001.

Inness, A., Ades, M., Agustí-Panareda, A., Barré, J., Benedictow, A., Blechschmidt, A.-M., Dominguez, J. J., Engelen, R., Eskes, H., Flemming, J., Huijnen, V., Jones, L., Kipling, Z., Massart, S., Parrington, M., Peuch, V.-H., Razinger, M., Remy, S., Schulz, M., and Suttie, M.: The CAMS reanalysis of atmospheric composition, Atmospheric Chemistry and Physics, 19, 3515–3556, https://doi.org/10.5194/acp-19-3515-2019, 2019.

Kalisa, W., Zhang, J., Igbawua, T., Henchiri, M., Mulinga, N., Nibagwire, D., and Umuhoza, M.: Spatial and temporal heterogeneity of air pollution in East Africa, Science of The Total Environment, 886, 163 734, https://doi.org/10.1016/j.scitotenv.2023.163734, 2023.

Kapsomenakis, J., Zerefos, C., Langerock, B., Errera, Q., Basart, S., Cuevas, E., Bennouna, Y., Thouret, V., Arola, A., Pitkänen, M., Blechschmidt, A.-M., Richter, A., Eskes, H., Tsikerdekis, T., Benedictow, A., Schulz, M., Bouarar, I., and Warneke, T.: Validation report of the CAMS global Reanalysis of aerosols and reactive gases, years 2003-2021 | Copernicus — atmosphere.copernicus.eu, https://atmosphere.copernicus.eu/node/789, [Accessed 29-03-2024], 2021.

Karypidou, M. C., Katragkou, E., and Sobolowski, S. P.: Precipitation over southern Africa: is there consensus among global climate models (GCMs), regional climate models (RCMs) and observational data?, Geosci. Model Dev., 15, 3387–3404, 2022.

Katoto, P. D., Byamungu, L., Brand, A. S., Mokaya, J., Strijdom, H., Goswami, N., De Boever, P., Nawrot, T. S., and Nemery, B.: Ambient air pollution and health in Sub-Saharan Africa: Current evidence, perspectives and a call to action., Environmental Research, 173, 174–188, https://doi.org/10.1016/j.envres.2019.03.029, 2019.

Kawamiya, M., Hajima, T., Tachiiri, K., Watanabe, S., and Yokohata, T.: Two decades of Earth system modeling with an emphasis on Model for Interdisciplinary Research on Climate (MIROC), Prog. Earth Planet. Sci., 7, 2020.

Kebede, A., Friberg, J., Isaxon, C., Jerrett, M., Malmqvist, E., Sjöström, C., Taj, T., and Vargas, A.: Air Quality in Africa: Public Health Implications, Annual Review of Public Health, 41, 193–210, https://doi.org/10.1146/annurev-publhealth100119-113802, 2021.

Kelley, M., Schmidt, G. A., Nazarenko, L. S., Bauer, S. E., Ruedy, R., Russell, G. L., Ackerman, A. S., Aleinov, I., Bauer, M., Bleck, R., Canuto, V., Cesana, G., Cheng, Y., Clune, T. L., Cook, B. I., Cruz, C. A., Del Genio, A. D., Elsaesser, G. S., Faluvegi, G., Kiang, N. Y., Kim, D., Lacis, A. A., Leboissetier, A., LeGrande, A. N., Lo, K. K., Marshall, J., Matthews, E. E., McDermid, S., Mezuman, K., Miller, R. L., Murray, L. T., Oinas, V., Orbe, C., García-Pando, C. P., Perlwitz, J. P., Puma, M. J., Rind, D., Romanou, A., Shindell, D. T., Sun, S., Tausnev, N., Tsigaridis, K., Tselioudis, G., Weng, E., Wu, J., and Yao, M.-S.: GISS-E2.1: Configurations and Climatology, Journal of Advances in Modeling Earth Systems, 12, e2019MS002 025, https://doi.org/https://doi.org/10.1029/2019MS002025, e2019MS002025 10.1029/2019MS002025, 2020.

Kim, Y., Noh, Y., Kim, D., Lee, M.-I., Lee, H. J., Kim, S. Y., and Kim, D.: KIOST KIOST-ESM model output prepared for CMIP6 CMIP historical, https://doi.org/10.22033/ESGF/CMIP6.5296, 2019.

Krasting, J. P., John, J. G., Blanton, C., McHugh, C., Nikonov, S., Radhakrishnan, A., Rand, K., Zadeh, N. T., Balaji, V., Durachta, J., Dupuis, C., Menzel, R., Robinson, T., Underwood, S., Vahlenkamp, H., Dunne, K. A., Gauthier, P. P., Ginoux, P., Griffies, S. M., Hallberg, R., Harrison, M., Hurlin, W., Malyshev, S., Naik, V., Paulot, F., Paynter, D. J., Ploshay, J., Reichl, B. G., Schwarzkopf, D. M., Seman, C. J., Silvers, L., Wyman, B., Zeng, Y., Adcroft, A., Dunne, J. P., Dussin, R., Guo, H., He, J., Held, I. M., Horowitz, L. W., Lin, P., Milly, P., Shevliakova, E., Stock, C., Winton, M., Wittenberg, A. T., Xie, Y., and Zhao, M.: NOAA-GFDL GFDL-ESM4 model output prepared for CMIP6 CMIP historical, https://doi.org/10.22033/ESGF/CMIP6.8597, 2018.

Krishnan, R., Swapna, P., Choudhury, A. D., Narayansetti, S., Prajeesh, A. G., Singh, M., Modi, A., Mathew, R., Vellore, R., Jyoti, J., Sabin, T. P., Sanjay, J., and Ingle, S.: The IITM Earth System Model (IITM ESM), 2021.

https://doi.org/10.5194/egusphere-2024-3057
Preprint. Discussion started: 23 October 2024

Kuhlbrodt, T., Jones, C. G., Sellar, A., Storkey, D., Blockley, E., Stringer, M., Hill, R., Graham, T., Ridley, J., Blaker, A., Calvert, D., Copsey, D., Ellis, R., Hewitt, H., Hyder, P., Ineson, S., Mulcahy, J., Siahaan, A., and Walton, J.: The Low-Resolution Version of HadGEM3 GC3.1: Development and Evaluation for Global Climate, Journal of Advances in Modeling Earth Systems, 10, 2865–2888, https://doi.org/https://doi.org/10.1029/2018MS001370, 2018.

Lavaysse, C., Flamant, C., Evan, A., Janicot, S., and Gaetani, M.: Recent climatological trend of the Saharan heat low and its impact on the West African climate, Clim. Dyn., 47, 3479–3498, 2016.

Lawrence, B. N., Bennett, V., Churchill, J., Juckes, M., Kershaw, P., Oliver, P., Pritchard, M., and Stephens, A.: The JASMIN super-data-cluster, https://doi.org/10.48550/ARXIV.1204.3553, 2012.

Lee, J., Hsu, N. C., Bettenhausen, C., and Sayer, A. M.: Retrieval of aerosol optical depth under thin cirrus from MODIS: Application to an ocean algorithm, Journal of Geophysical Research: Atmospheres, 118, https://doi.org/10.1002/jgrd.50806, 2013.

Lee, J., Kim, J., Sun, M.-A., Kim, B.-H., Moon, H., Sung, H. M., Kim, J., and Byun, Y.-H.: Evaluation of the Korea Meteorological Administration Advanced Community Earth-System model (K-ACE), Asia-Pacific Journal of Atmospheric Sciences, 56, 381–395, https://doi.org/10.1007/s13143-019-00144-7, 2020.

Lee, W.-L. and Liang, H.-C.: AS-RCEC TaiESM1.0 model output prepared for CMIP6 CMIP historical, 2020.

Levin, Z. and Cotton, W. R., eds.: Aerosol pollution impact on precipitation, Springer, New York, NY, 2009 edn., 2008.

Li, L.: CAS FGOALS-g3 model output prepared for CMIP6 CMIP historical, https://doi.org/10.22033/ESGF/CMIP6.3356, 2019.

Li, L., Yu, Y., Tang, Y., Lin, P., Xie, J., Song, M., Dong, L., Zhou, T., Liu, L., Wang, L., Pu, Y., Chen, X., Chen, L., Xie, Z., Liu, H., Zhang, L., Huang, X., Feng, T., Zheng, W., Xia, K., Liu, H., Liu, J., Wang, Y., Wang, L., Jia, B., Xie, F., Wang, B., Zhao, S., Yu, Z., Zhao, B., and Wei, J.: The Flexible Global Ocean-Atmosphere-Land System Model Grid-Point Version 3 (FGOALS-g3): Description and Evaluation, Journal of Advances in Modeling Earth Systems, 12, e2019MS002 012, https://doi.org/https://doi.org/10.1029/2019MS002012, e2019MS002012 2019MS002012, 2020.

Lin, Y., Huang, X., Liang, Y., Qin, Y., Xu, S., Huang, W., Xu, F., Liu, L., Wang, Y., Peng, Y., Wang, L., Xue, W., Fu, H., Zhang, G. J., Wang, B., Li, R., Zhang, C., Lu, H., Yang, K., Luo, Y., Bai, Y., Song, Z., Wang, M., Zhao, W., Zhang, F., Xu, J., Zhao, X., Lu, C., Chen, Y., Luo, Y., Hu, Y., Tang, Q., Chen, D., Yang, G., and Gong, P.: Community Integrated Earth System Model (CIESM): Description and Evaluation, Journal of Advances in Modeling Earth Systems, 12, e2019MS002 036, https://doi.org/https://doi.org/10.1029/2019MS002036, e2019MS002036 2019MS002036, 2020.

Lovato, T. and Peano, D.: CMCC CMCC-CM2-SR5 model output prepared for CMIP6 CMIP historical, https://doi.org/10.22033/ESGF/CMIP6.3825, 2020.

Lüdecke, H.-J., Müller-Plath, G., Wallace, M. G., and Lüning, S.: Decadal and multidecadal natural variability of African rainfall, Journal of Hydrology: Regional Studies, 34, 100 795, https://doi.org/10.1016/j.ejrh.2021.100795, 2021.

Lund, M. T., Myhre, G., and Samset, B. H.: Anthropogenic aerosol forcing under the Shared Socioeconomic Pathways, Atmospheric Chemistry and Physics, 19, 13 827–13 839, https://doi.org/10.5194/acp-19-13827-2019, 2019.

Lund, M. T., Myhre, G., Skeie, R. B., Samset, B. H., and Klimont, Z.: Implications of differences between recent anthropogenic aerosol emission inventories for diagnosed AOD and radiative forcing from 1990 to 2019, Atmospheric Chemistry and Physics, 23, 6647–6662, https://doi.org/10.5194/acp-23-6647-2023, 2023.

McFarlane, C., Isevulambire, P. K., Lumbuenamo, R. S., Ndinga, A. M. E., Dhammapala, R., Jin, X., McNeill, V. F., Malings, C., Subramanian, R., and Westervelt, D. M.: First Measurements of Ambient PM2.5 in Kinshasa, Democratic Republic of Congo

https://doi.org/10.5194/egusphere-2024-3057
Preprint. Discussion started: 23 October 2024

and Brazzaville, Republic of Congo Using Field-calibrated Low-cost Sensors, Aerosol and Air Quality Research, 21, 200 619, https://doi.org/10.4209/aaqr.200619, 2021.

Miller, R. L., Schmidt, G. A., Nazarenko, L. S., Bauer, S. E., Kelley, M., Ruedy, R., Russell, G. L., Ackerman, A. S., Aleinov, I., Bauer, M., Bleck, R., Canuto, V., Cesana, G., Cheng, Y., Clune, T. L., Cook, B. I., Cruz, C. A., Del Genio, A. D., Elsaesser, G. S., Faluvegi, G., Kiang, N. Y., Kim, D., Lacis, A. A., Leboissetier, A., LeGrande, A. N., Lo, K. K., Marshall, J., Matthews, E. E., McDermid, S., Mezuman, K., Murray, L. T., Oinas, V., Orbe, C., Pérez García-Pando, C., Perlwitz, J. P., Puma, M. J., Rind, D., Romanou, A., Shindell, D. T., Sun, S., Tausnev, N., Tsigaridis, K., Tselioudis, G., Weng, E., Wu, J., and Yao, M.-S.: CMIP6 Historical Simulations (1850–2014) With GISS-E2.1, Journal of Advances in Modeling Earth Systems, 13, e2019MS002 034, https://doi.org/https://doi.org/10.1029/2019MS002034, e2019MS002034 10.1029/2019MS002034, 2021.

Mitchell, T. D. and Jones, P. D.: An improved method of constructing a database of monthly climate observations and associated high-resolution grids, Int. J. Climatol., 25, 693–712, 2005.

Monerie, P., Dittus, A. J., Wilcox, L. J., and Turner, A. G.: Uncertainty in Simulating Twentieth Century West African Precipitation Trends: The Role of Anthropogenic Aerosol Emissions, Earth's Future, 11, https://doi.org/10.1029/2022ef002995, 2023.

Mulcahy, J. P., Jones, C. G., Rumbold, S. T., Kuhlbrodt, T., Dittus, A. J., Blockley, E. W., Yool, A., Walton, J., Hardacre, C., Andrews, T., Bodas-Salcedo, A., Stringer, M., de Mora, L., Harris, P., Hill, R., Kelley, D., Robertson, E., and Tang, Y.: UKESM1.1: development and evaluation of an updated configuration of the UK Earth System Model, Geoscientific Model Development, 16, 1569–1600, https://doi.org/10.5194/gmd-16-1569-2023, 2023.

Munday, C., Washington, R., and Hart, N.: African Low-Level Jets and Their Importance for Water Vapor Transport and Rainfall, Geophysical Research Letters, 48, https://doi.org/10.1029/2020gl090999, 2021.

Munday, C., Engelstaedter, S., Ouma, G., Ogutu, G., Olago, D., Ong'ech, D., Lees, T., Wanguba, B., Nkatha, R., Ogolla, C., Gàlgalo, R. A., Dokata, A. J., Kirui, E., Hope, R., and Washington, R.: Observations of the Turkana Jet and the East African Dry Tropics: The RIFTJet Field Campaign, Bulletin of the American Meteorological Society, 103, E1828–E1842, https://doi.org/10.1175/bams-d-21-0214.1, 2022.

Myhre, G., Lund Myhre, C., Samset, B. H., and Storelvmo, T.: Aerosols and their Relation to Global Climate and Climate Sensitivity, Nature Education Knowledge, 4, 7, 2013.

Narayanasetti, S., Panickal, S., Raghavan, K., Gopinathan, P. A., Choudhury, A. D., and Singh, M.: CCCR-IITM IITM-ESM model output prepared for CMIP6 CMIP piControl, 2019.

NASA GISS: NASA-GISS GISS-E2-2-G model output prepared for CMIP6 CMIP amip, 2019a.

NASA GISS: NASA-GISS GISS-E2.2H model output prepared for CMIP6 CMIP piControl, 2019b.

Neubauer, D., Ferrachat, S., Siegenthaler-Le Drian, C., Stoll, J., Folini, D. S., Tegen, I., Wieners, K.-H., Mauritsen, T., Stemmler, I., Barthel, S., Bey, I., Daskalakis, N., Heinold, B., Kokkola, H., Partridge, D., Rast, S., Schmidt, H., Schutgens, N., Stanelle, T., Stier, P., Watson-Parris, D., and Lohmann, U.: HAMMOZ-Consortium MPI-ESM1.2-HAM model output prepared for CMIP6 AerChemMIP, https://doi.org/10.22033/ESGF/CMIP6.1621, 2019.

Niang, C., Mancho, A. M., García-Garrido, V. J., Mohino, E., Rodriguez-Fonseca, B., and Curbelo, J.: Transport pathways across the West African Monsoon as revealed by Lagrangian Coherent Structures, Scientific Reports, 10, https://doi.org/10.1038/s41598-020-69159-9, 2020.

O'Neill, B. C., Tebaldi, C., van Vuuren, D. P., Eyring, V., Friedlingstein, P., Hurtt, G., Knutti, R., Kriegler, E., Lamarque, J.-F., Lowe, J., Meehl, G. A., Moss, R., Riahi, K., and Sanderson, B. M.: The Scenario Model Intercomparison Project (ScenarioMIP) for CMIP6, Geosci. Model Dev., 9, 3461–3482, 2016.

https://doi.org/10.5194/egusphere-2024-3057
Preprint. Discussion started: 23 October 2024

Pak, G., Noh, Y., Lee, M.-I., Yeh, S.-W., Kim, D., Kim, S.-Y., Lee, J.-L., Lee, H. J., Hyun, S.-H., Lee, K.-Y., Lee, J.-H., Park, Y.-G., Jin, H., Park, H., and Kim, Y. H.: Korea Institute of Ocean Science and Technology Earth System Model and Its Simulation Characteristics, Ocean Science Journal, 56, 18–45, https://doi.org/10.1007/s12601-021-00001-7, 2021.

Peano, D., Lovato, T., and Materia, S.: CMCC CMCC-ESM2 model output prepared for CMIP6 LS3MIP, 2020.

Persad, G. G.: The dependence of aerosols' global and local precipitation impacts on the emitting region, Atmos. Chem. Phys., 23, 3435–3452, 2023.

Peterson, P., Funk, C., Landsfeld, M., Husak, G., Pedreros, D., Verdin, J., Rowland, J., Shukla, S., McNally, A., Michaelsen, J., and Verdin, A.: The Climate Hazards Group Infrared Precipitation with Stations (CHIRPS) Dataset: Quasi-Global Precipitation Estimates for Drought Monitoring and Trend Analysis — agu.confex.com, https://agu.confex.com/agu/fm14/meetingapp.cgi/Paper/8104, 2014.

Porkka, M., Wang-Erlandsson, L., Destouni, G., Ekman, A. M. L., Rockström, J., and Gordon, L. J.: Is wetter better? Exploring agriculturally-relevant rainfall characteristics over four decades in the Sahel, Environmental Research Letters, 16, 035 002, https://doi.org/10.1088/1748-9326/abdd57, 2021.

Raheja, G., Nimo, J., Appoh, E. K.-E., Essien, B., Sunu, M., Nyante, J., Amegah, M., Quansah, R., Arku, R. E., Penn, S. L., Giordano, M. R., Zheng, Z., Jack, D., Chillrud, S., Amegah, K., Subramanian, R., Pinder, R., Appah-Sampong, E., Tetteh, E. N., Borketey, M. A., Hughes, A. F., and Westervelt, D. M.: Low-Cost Sensor Performance Intercomparison, Correction Factor Development, and 2+ Years of Ambient PM2.5 Monitoring in Accra, Ghana, Environmental Science & Technology, 57, 10 708–10 720, https://doi.org/10.1021/acs.est.2c09264, 2023.

Ramanathan, V. and Carmichael, G.: Global and regional climate changes due to black carbon, Nat. Geosci., 1, 221–227, 2008.

Reddington, C. L., Spracklen, D. V., Artaxo, P., Ridley, D. A., Rizzo, L. V., and Arana, A.: Analysis of particulate emissions from tropical biomass burning using a global aerosol model and long-term surface observations, Atmospheric Chemistry and Physics, 16, 11 083–11 106, https://doi.org/10.5194/acp-16-11083-2016, 2016.

Ridley, J., Menary, M., Kuhlbrodt, T., Andrews, M., and Andrews, T.: MOHC HadGEM3-GC31-LL model output prepared for CMIP6 CMIP historical, https://doi.org/10.22033/ESGF/CMIP6.6109, 2019a.

Ridley, J., Menary, M., Kuhlbrodt, T., Andrews, M., and Andrews, T.: MOHC HadGEM3-GC31-MM model output prepared for CMIP6 CMIP historical, https://doi.org/10.22033/ESGF/CMIP6.6112, 2019b.

Rind, D., Orbe, C., Jonas, J., Nazarenko, L., Zhou, T., Kelley, M., Lacis, A., Shindell, D., Faluvegi, G., Romanou, A., Russell, G., Tausnev, N., Bauer, M., and Schmidt, G.: GISS model E2.2: A climate model optimized for the middle atmosphere—model structure, climatology, variability, and climate sensitivity, J. Geophys. Res., 125, 2020.

Rong, X.: CAMS CAMS_CSM1.0 model output prepared for CMIP6 CMIP historical, https://doi.org/10.22033/ESGF/CMIP6.9754, 2019.

Samset, B. H.: Aerosol absorption has an underappreciated role in historical precipitation change, Communications Earth & Environment, 3, https://doi.org/10.1038/s43247-022-00576-6, 2022.

Samset, B. H., Sand, M., Smith, C. J., Bauer, S. E., Forster, P. M., Fuglestvedt, J. S., Osprey, S., and Schleussner, C.: Climate Impacts From a Removal of Anthropogenic Aerosol Emissions, Geophysical Research Letters, 45, 1020–1029, https://doi.org/10.1002/2017gl076079, 2018.

Scannell, C., Booth, B. B. B., Dunstone, N. J., Rowell, D. P., Bernie, D. J., Kasoar, M., Voulgarakis, A., Wilcox, L. J., Acosta Navarro, J. C., Seland, . y., and Paynter, D. J.: The Influence of Remote Aerosol Forcing from Industrialized Economies on the Future Evolution of East and West African Rainfall, Journal of Climate, 32, 8335–8354, https://doi.org/10.1175/jcli-d-18-0716.1, 2019.

https://doi.org/10.5194/egusphere-2024-3057
Preprint. Discussion started: 23 October 2024

Schutgens, N. A. J., Gryspeerdt, E., Weigum, N., Tsyro, S., Goto, D., Schulz, M., and Stier, P.: Will a perfect model agree with perfect observations? The impact of spatial sampling, Atmospheric Chemistry and Physics, 16, 6335–6353, https://doi.org/10.5194/acp-16-6335-2016, 2016.

Schwarzwald, K., Goddard, L., Seager, R., Ting, M., and Marvel, K.: Understanding CMIP6 biases in the representation of the Greater Horn of Africa long and short rains, Climate Dynamics, 61, 1229–1255, https://doi.org/10.1007/s00382-022-06622-5, 2022.

Schwarzwald, K., Goddard, L., Seager, R., Ting, M., and Marvel, K.: Understanding CMIP6 biases in the representation of the greater Horn of Africa long and short rains, Climate Dynamics, 61, 1229–1255, https://doi.org/10.1007/s00382-022-06622-5, 2023.

Scoccimarro, E., Bellucci, A., and Peano, D.: CMCC CMCC-CM2-HR4 model output prepared for CMIP6 CMIP historical, https://doi.org/10.22033/ESGF/CMIP6.3823, 2020.

Seferian, R.: CNRM-CERFACS CNRM-ESM2-1 model output prepared for CMIP6 CMIP historical, https://doi.org/10.22033/ESGF/CMIP6.4068, 2018.

Séférian, R., Nabat, P., Michou, M., Saint-Martin, D., Voldoire, A., Colin, J., Decharme, B., Delire, C., Berthet, S., Chevallier, M., Sénési, S., Franchisteguy, L., Vial, J., Mallet, M., Joetzjer, E., Geoffroy, O., Guérémy, J.-F., Moine, M.-P., Msadek, R., Ribes, A., Rocher, M., Roehrig, R., Salas-y Mélia, D., Sanchez, E., Terray, L., Valcke, S., Waldman, R., Aumont, O., Bopp, L., Deshayes, J., Éthé, C., and Madec, G.: Evaluation of CNRM Earth System Model, CNRM-ESM2-1: Role of Earth System Processes in Present-Day and Future Climate, Journal of Advances in Modeling Earth Systems, 11, 4182–4227, https://doi.org/https://doi.org/10.1029/2019MS001791, 2019.

Seinfeld, J. H. and Pandis, S. N.: Atmospheric chemistry and physics, Wiley-Blackwell, Hoboken, NJ, 3 edn., 2016.

Seland, Ø., Bentsen, M., Olivié, D., Toniazzo, T., Gjermundsen, A., Graff, L. S., Debernard, J. B., Gupta, A. K., He, Y.-C., Kirkevåg, A., Schwinger, J., Tjiputra, J., Aas, K. S., Bethke, I., Fan, Y., Griesfeller, J., Grini, A., Guo, C., Ilicak, M., Karset, I. H. H., Landgren, O., Liakka, J., Moseid, K. O., Nummelin, A., Spensberger, C., Tang, H., Zhang, Z., Heinze, C., Iversen, T., and Schulz, M.: Overview of the Norwegian Earth System Model (NorESM2) and key climate response of CMIP6 DECK, historical, and scenario simulations, Geoscientific Model Development, 13, 6165–6200, https://doi.org/10.5194/gmd-13-6165-2020, 2020.

Seland, y., Bentsen, M., Oliviè, D. J. L., Toniazzo, T., Gjermundsen, A., Graff, L. S., Debernard, J. B., Gupta, A. K., He, Y., Kirkevåg, A., Schwinger, J., Tjiputra, J., Aas, K. S., Bethke, I., Fan, Y., Griesfeller, J., Grini, A., Guo, C., Ilicak, M., Karset, I. H. H., Landgren, O. A., Liakka, J., Moseid, K. O., Nummelin, A., Spensberger, C., Tang, H., Zhang, Z., Heinze, C., Iversen, T., and Schulz, M.: NCC NorESM2-LM model output prepared for CMIP6 CMIP historical, https://doi.org/10.22033/ESGF/CMIP6.8036, 2019.

Sellar, A. A., Jones, C. G., Mulcahy, J. P., Tang, Y., Yool, A., Wiltshire, A., O'Connor, F. M., Stringer, M., Hill, R., Palmieri, J., Woodward, S., de Mora, L., Kuhlbrodt, T., Rumbold, S. T., Kelley, D. I., Ellis, R., Johnson, C. E., Walton, J., Abraham, N. L., Andrews, M. B., Andrews, T., Archibald, A. T., Berthou, S., Burke, E., Blockley, E., Carslaw, K., Dalvi, M., Edwards, J., Folberth, G. A., Gedney, N., Griffiths, P. T., Harper, A. B., Hendry, M. A., Hewitt, A. J., Johnson, B., Jones, A., Jones, C. D., Keeble, J., Liddicoat, S., Morgenstern, O., Parker, R. J., Predoi, V., Robertson, E., Siahaan, A., Smith, R. S., Swaminathan, R., Woodhouse, M. T., Zeng, G., and Zerroukat, M.: UKESM1: Description and Evaluation of the U.K. Earth System Model, Journal of Advances in Modeling Earth Systems, 11, 4513–4558, https://doi.org/https://doi.org/10.1029/2019MS001739, 2019.

Semmler, T., Danilov, S., Rackow, T., Sidorenko, D., Barbi, D., Hegewald, J., Sein, D., Wang, Q., and Jung, T.: AWI AWI-CM1.1MR model output prepared for CMIP6 CMIP, https://doi.org/10.22033/ESGF/CMIP6.359, 2018.

Semmler, T., Danilov, S., Gierz, P., Goessling, H. F., Hegewald, J., Hinrichs, C., Koldunov, N., Khosravi, N., Mu, L., Rackow, T., Sein, D. V., Sidorenko, D., Wang, Q., and Jung, T.: Simulations for CMIP6 With the AWI Climate Model AWI-CM-1-1, Journal of Advances in Modeling Earth Systems, 12, https://doi.org/10.1029/2019ms002009, 2020.

https://doi.org/10.5194/egusphere-2024-3057
Preprint. Discussion started: 23 October 2024

Senghor, H., Machu, E., Hourdin, F., and Gaye, A. T.: Seasonal cycle of desert aerosols in western Africa: analysis of the coastal transition with passive and active sensors, Atmospheric Chemistry and Physics, 17, 8395–8410, https://doi.org/10.5194/acp-17-8395-2017, 2017.

Sepulchre, P., Caubel, A., Ladant, J.-B., Bopp, L., Boucher, O., Braconnot, P., Brockmann, P., Cozic, A., Donnadieu, Y., Estella-Perez, V., Ethé, C., Fluteau, F., Foujols, M.-A., Gastineau, G., Ghattas, J., Hauglustaine, D., Hourdin, F., Kageyama, M., Khodri, M., Marti, O., Meurdesoif, Y., Mignot, J., Sarr, A.-C., Servonnat, J., Swingedouw, D., Szopa, S., and Tardif, D.: IPSL-CM5A2. An Earth System Model designed for multi-millennial climate simulations, 2019.

Shindell, D., Faluvegi, G., Parsons, L., Nagamoto, E., and J., C.: Premature deaths in Africa due to particulate matter under high and low warming scenarios, GeoHealth, 6, e2022GH000 601, https://doi.org/10.1029/2022GH000601, 2022.

Shindell, D., Parsons, L., Faluvegi, G., Hicks, K., Kuylenstierna, J., and Heaps, C.: The important role of African emissions reductions in projected local rainfall changes, Npj Clim. Atmos. Sci., 6, 2023.

Sidorenko, D., Rackow, T., Jung, T., Semmler, T., Barbi, D., Danilov, S., Dethloff, K., Dorn, W., Fieg, K., Goessling, H. F., Handorf, D., Harig, S., Hiller, W., Juricke, S., Losch, M., Schröter, J., Sein, D. V., and Wang, Q.: Towards multi-resolution global climate modeling with ECHAM6–FESOM. Part I: model formulation and mean climate, Climate Dynamics, 44, 757–780, https://doi.org/10.1007/s00382-014-2290-6, 2015.

Stier, P., van den Heever, S. C., Christensen, M. W., Gryspeerdt, E., Dagan, G., Saleeby, S. M., Bollasina, M., Donner, L., Emanuel, K., Ekman, A. M. L., Feingold, G., Field, P., Forster, P., Haywood, J., Kahn, R., Koren, I., Kummerow, C., L'Ecuyer, T., Lohmann, U., Ming, Y., Myhre, G., Quaas, J., Rosenfeld, D., Samset, B., Seifert, A., Stephens, G., and Tao, W.-K.: Multifaceted aerosol effects on precipitation, Nature Geoscience, 17, 719–732, https://doi.org/10.1038/s41561-024-01482-6, 2024.

Stouffer, R.: UA MCM-UA-1-0 model output prepared for CMIP6 ScenarioMIP ssp370, 2019.

Swart, N. C., Cole, J. N., Kharin, V. V., Lazare, M., Scinocca, J. F., Gillett, N. P., Anstey, J., Arora, V., Christian, J. R., Jiao, Y., Lee, W. G., Majaess, F., Saenko, O. A., Seiler, C., Seinen, C., Shao, A., Solheim, L., von Salzen, K., Yang, D., Winter, B., and Sigmond, M.: CCCma CanESM5 model output prepared for CMIP6 CMIP historical, https://doi.org/10.22033/ESGF/CMIP6.3610, 2019a.

Swart, N. C., Cole, J. N., Kharin, V. V., Lazare, M., Scinocca, J. F., Gillett, N. P., Anstey, J., Arora, V., Christian, J. R., Jiao, Y., Lee, W. G., Majaess, F., Saenko, O. A., Seiler, C., Seinen, C., Shao, A., Solheim, L., von Salzen, K., Yang, D., Winter, B., and Sigmond, M.: CCCma CanESM5-CanOE model output prepared for CMIP6 CMIP, https://doi.org/10.22033/ESGF/CMIP6.10205, 2019b.

Swart, N. C., Cole, J. N., Kharin, V. V., Lazare, M., Scinocca, J. F., Gillett, N. P., Anstey, J., Arora, V., Christian, J. R., Jiao, Y., Lee, W. G., Majaess, F., Saenko, O. A., Seiler, C., Seinen, C., Shao, A., Solheim, L., von Salzen, K., Yang, D., Winter, B., Sigmond, M., Abraham, C., Akingunola, A., and Reader, C.: CCCma CanESM5.1 model output prepared for CMIP6 CMIP, https://doi.org/10.22033/ESGF/CMIP6.17184, 2019c.

Swart, N. C., Cole, J. N. S., Kharin, V. V., Lazare, M., Scinocca, J. F., Gillett, N. P., Anstey, J., Arora, V., Christian, J. R., Hanna, S., Jiao, Y., Lee, W. G., Majaess, F., Saenko, O. A., Seiler, C., Seinen, C., Shao, A., Sigmond, M., Solheim, L., von Salzen, K., Yang, D., and Winter, B.: The Canadian Earth System Model version 5 (CanESM5.0.3), Geoscientific Model Development, 12, 4823–4873, https://doi.org/10.5194/gmd-12-4823-2019, 2019d.

Sylla, M. B., Giorgi, F., Coppola, E., and Mariotti, L.: Uncertainties in daily rainfall over Africa: assessment of gridded observation products and evaluation of a regional climate model simulation, Int. J. Climatol., 33, 1805–1817, 2013.

Tang, Y., Rumbold, S., Ellis, R., Kelley, D., Mulcahy, J., Sellar, A., Walton, J., and Jones, C.: MOHC UKESM1.0-LL model output prepared for CMIP6 CMIP historical, https://doi.org/10.22033/ESGF/CMIP6.6113, 2019.

https://doi.org/10.5194/egusphere-2024-3057
Preprint. Discussion started: 23 October 2024

Tatebe, H. and Watanabe, M.: MIROC MIROC6 model output prepared for CMIP6 CMIP historical, https://doi.org/10.22033/ESGF/CMIP6.5603, 2018.

Tatebe, H., Ogura, T., Nitta, T., Komuro, Y., Ogochi, K., Takemura, T., Sudo, K., Sekiguchi, M., Abe, M., Saito, F., Chikira, M., Watanabe, S., Mori, M., Hirota, N., Kawatani, Y., Mochizuki, T., Yoshimura, K., Takata, K., O'ishi, R., Yamazaki, D., Suzuki, T., Kurogi, M., Kataoka, T., Watanabe, M., and Kimoto, M.: Description and basic evaluation of simulated mean state, internal variability, and climate sensitivity in MIROC6, Geoscientific Model Development, 12, 2727–2765, https://doi.org/10.5194/gmd-12-2727-2019, 2019.

Tramblay, Y. and Villarini, G.: Flood trends in Africa, https://doi.org/10.5194/egusphere-egu2020-7104, 2020.

Turnock, S. T., Allen, R. J., Andrews, M., Bauer, S. E., Deushi, M., Emmons, L., Good, P., Horowitz, L., John, J. G., Michou, M., Nabat, P., Naik, V., Neubauer, D., O'Connor, F. M., Olivié, D., Oshima, N., Schulz, M., Sellar, A., Shim, S., Takemura, T., Tilmes, S., Tsigaridis, K., Wu, T., and Zhang, J.: Historical and future changes in air pollutants from CMIP6 models, Atmospheric Chemistry and Physics, 20, 14 547–14 579, https://doi.org/10.5194/acp-20-14547-2020, 2020.

Twomey, S.: The Influence of Pollution on the Shortwave Albedo of Clouds, Journal of the Atmospheric Sciences, 34, 1149–1152, https://doi.org/10.1175/1520-0469(1977)034<1149:tiopot>2.0.co;2, 1977.

Twomey, S. A., Piepgrass, M., and Wolfe, T. L.: An assessment of the impact of pollution on global cloud albedo, Tellus B, 36B, 356–366, https://doi.org/10.1111/j.1600-0889.1984.tb00254.x, 1984.

U. S. Environmental Protection Agency: REFERENCE AND EQUIVALENT METHOD APPLICATIONS, https://www.epa.gov/sites/default/files/2017-02/documents/frmfemguidelines.pdf, [Accessed 06-08-2024], 2011.

United Nations Environment Programme: Global environment outlook 6 (GEO-6), United Nations Environment Programme, Genève, Switzerland, 2017.

Voldoire, A.: CMIP6 simulations of the CNRM-CERFACS based on CNRM-CM6-1 model for CMIP experiment historical, https://doi.org/10.22033/ESGF/CMIP6.4066, 2018.

Voldoire, A.: CNRM-CERFACS CNRM-CM6-1-HR model output prepared for CMIP6 ScenarioMIP ssp585, 2019.

Voldoire, A., Saint-Martin, D., Sénési, S., Decharme, B., Alias, A., Chevallier, M., Colin, J., Guérémy, J.-F., Michou, M., Moine, M.-P., Nabat, P., Roehrig, R., Salas y Mélia, D., Séférian, R., Valcke, S., Beau, I., Belamari, S., Berthet, S., Cassou, C., Cattiaux, J., Deshayes, J., Douville, H., Ethé, C., Franchistéguy, L., Geoffroy, O., Lévy, C., Madec, G., Meurdesoif, Y., Msadek, R., Ribes, A., Sanchez-Gomez, E., Terray, L., and Waldman, R.: Evaluation of CMIP6 DECK Experiments With CNRM-CM6-1, Journal of Advances in Modeling Earth Systems, 11, 2177–2213, https://doi.org/https://doi.org/10.1029/2019MS001683, 2019.

Volodin, E., Mortikov, E., Gritsun, A., Lykossov, V., Galin, V., Diansky, N., Gusev, A., Kostrykin, S., Iakovlev, N., Shestakova, A., and Emelina, S.: INM INM-CM4-8 model output prepared for CMIP6 CMIP historical, https://doi.org/10.22033/ESGF/CMIP6.5069, 2019a.

Volodin, E., Mortikov, E., Gritsun, A., Lykossov, V., Galin, V., Diansky, N., Gusev, A., Kostrykin, S., Iakovlev, N., Shestakova, A., and Emelina, S.: INM INM-CM5-0 model output prepared for CMIP6 CMIP historical, https://doi.org/10.22033/ESGF/CMIP6.5070, 2019b.

Volodin, E. M. and Kostrykin, S. V.: The aerosol module in the INM RAS climate model, Russian Meteorology and Hydrology, 41, 519–528, https://doi.org/10.3103/S106837391608001X, 2016.

Volodin, E. M., Dianskii, N. A., and Gusev, A. V.: Simulating present-day climate with the INMCM4.0 coupled model of the atmospheric and oceanic general circulations, Izvestiya, Atmospheric and Oceanic Physics, 46, 414–431, https://doi.org/10.1134/S000143381004002X, 2010.

https://doi.org/10.5194/egusphere-2024-3057
Preprint. Discussion started: 23 October 2024

Volodin, E. M., Mortikov, E. V., Kostrykin, S. V., Galin, V. Y., Lykossov, V. N., Gritsun, A. S., Diansky, N. A., Gusev, A. V., and Iakovlev, N. G.: Simulation of the present-day climate with the climate model INMCM5, Climate Dynamics, 49, 3715–3734, https://doi.org/10.1007/s00382-017-3539-7, 2017.

Wagner, S. C., Govaerts, Y. M., and Lattanzio, A.: Joint retrieval of surface reflectance and aerosol optical depth from MSG/SEVIRI observations with an optimal estimation approach: 2. Implementation and evaluation, J. Geophys. Res., 115, 2010.

Walton, J., Mulcahy, J., Tang, Y., Rumbold, S., Hardacre, C., Stringer, M., Hill, R., Kuhlbrodt, T., and Jones, C.: MOHC UKESM1.1-LL model output prepared for CMIP6 ScenarioMIP, 2022.

Wang, R., Cui, K., Sheu, H.-L., Wang, L.-C., and Liu, X.: Effects of Precipitation on the Air Quality Index, PM2.5 Levels and on the Dry Deposition of PCDD/Fs in the Ambient Air, Aerosol and Air Quality Research, 23, 220 417, https://doi.org/10.4209/aaqr.220417, 2023.

Wang, Y.-C., Hsu, H.-H., Chen, C.-A., Tseng, W.-L., Hsu, P.-C., Lin, C.-W., Chen, Y.-L., Jiang, L.-C., Lee, Y.-C., Liang, H.-C., Chang, W.-M., Lee, W.-L., and Shiu, C.-J.: Performance of the Taiwan Earth System Model in simulating climate variability compared with observations and CMIP6 model simulations, J. Adv. Model. Earth Syst., 13, 2021.

Watanabe, S., Hajima, T., Sudo, K., Abe, M., Arakawa, O., Ogochi, K., Arakawa, T., Tatebe, H., Ito, A., Ito, A., Komuro, Y., Nitta, T., Noguchi, M. A., Ogura, T., Ohgaito, R., Sekiguchi, M., Suzuki, T., Tachiiri, K., Takata, K., Takemura, T., Watanabe, M., Yamamoto, A., Yamazaki, D., Yoshimura, K., and Kawamiya, M.: MIROC MIROC-ES2H model output prepared for CMIP6 GeoMIP, 2021.

Wei, G., Sun, P., Jiang, S., Shen, Y., Liu, B., Zhang, Z., and Ouyang, X.: The Driving Influence of Multi-Dimensional Urbanization on PM2.5 Concentrations in Africa: New Evidence from Multi-Source Remote Sensing Data, 2000–2018, International Journal of Environmental Research and Public Health, 18, 9389, https://doi.org/10.3390/ijerph18179389, 2021.

Wells, C. D., Kasoar, M., Bellouin, N., and Voulgarakis, A.: Local and remote climate impacts of future African aerosol emissions, Atmos. Chem. Phys., 23, 3575–3593, 2023.

Westervelt, D. M., Conley, A. J., Fiore, A. M., Lamarque, J., Shindell, D., Previdi, M., Faluvegi, G., Correa, G., and Horowitz, L. W.: Multimodel precipitation responses to removal of U.S. sulfur dioxide emissions, Journal of Geophysical Research: Atmospheres, 122, 5024–5038, https://doi.org/10.1002/2017jd026756, 2017.

Westervelt, D. M., Mascioli, N. R., Fiore, A. M., Conley, A. J., Lamarque, J.-F., Shindell, D. T., Faluvegi, G., Previdi, M., Correa, G., and Horowitz, L. W.: Local and remote mean and extreme temperature response to regional aerosol emissions reductions, Atmospheric Chemistry and Physics, 20, 3009–3027, https://doi.org/10.5194/acp-20-3009-2020, 2020.

Westervelt, D. M., Isevulambire, P. K., Yombo Phaka, R., Yang, L. H., Raheja, G., Milly, G., Selenge, J.-L. B., Mulumba, J. P. M., Bousiotis, D., Djibi, B. L., McNeill, V. F., Ng, N. L., Pope, F., Mbela, G. K., and Konde, J. N.: Low-Cost Investigation into Sources of PM2.5 in Kinshasa, Democratic Republic of the Congo, ACS ES& T Air, 1, 43–51, https://doi.org/10.1021/acsestair.3c00024, 2023.

Wilcox, L. J., Allen, R. J., Samset, B. H., Bollasina, M. A., Griffiths, P. T., Keeble, J., Lund, M. T., Makkonen, R., Merikanto, J., O'Donnell, D., Paynter, D. J., Persad, G. G., Rumbold, S. T., Takemura, T., Tsigaridis, K., Undorf, S., and Westervelt, D. M.: The Regional Aerosol Model Intercomparison Project (RAMIP), Geoscientific Model Development, 16, 4451–4479, https://doi.org/10.5194/gmd-16-4451-2023, 2023.

Williams, A. I. L., Watson-Parris, D., Dagan, G., and Stier, P.: Dependence of Fast Changes in Global and Local Precipitation on the Geographical Location of Absorbing Aerosol, Journal of Climate, 36, 6163–6176, https://doi.org/10.1175/jcli-d-23-0022.1, 2023.

Woodward, S., Sellar, A. A., Tang, Y., Stringer, M., Yool, A., Robertson, E., and Wiltshire, A.: The simulation of mineral dust in the United Kingdom Earth System Model UKESM1, Atmospheric Chemistry and Physics, 22, 14 503–14 528, https://doi.org/10.5194/acp-22-14503-2022, 2022.

https://doi.org/10.5194/egusphere-2024-3057
Preprint. Discussion started: 23 October 2024

World Health Organisation: Drought and food insecurity in the greater Horn of Africa — who.int, https://www.who.int/emergencies/situations/drought-food-insecurity-greater-horn-of-africa, [Accessed 30-05-2024], 2024.

Wu, T., Chu, M., Dong, M., Fang, Y., Jie, W., Li, J., Li, W., Liu, Q., Shi, X., Xin, X., Yan, J., Zhang, F., Zhang, J., Zhang, L., and Zhang, Y.: BCC BCC-CSM2MR model output prepared for CMIP6 CMIP historical, https://doi.org/10.22033/ESGF/CMIP6.2948, 2018.

Wu, T., Lu, Y., Fang, Y., Xin, X., Li, L., Li, W., Jie, W., Zhang, J., Liu, Y., Zhang, L., Zhang, F., Zhang, Y., Wu, F., Li, J., Chu, M., Wang, Z., Shi, X., Liu, X., Wei, M., Huang, A., Zhang, Y., and Liu, X.: The Beijing Climate Center Climate System Model (BCC-CSM): the main progress from CMIP5 to CMIP6, Geoscientific Model Development, 12, 1573–1600, https://doi.org/10.5194/gmd-12-1573-2019, 2019.

Wu, T., Zhang, F., Zhang, J., Jie, W., Zhang, Y., Wu, F., Li, L., Yan, J., Liu, X., Lu, X., Tan, H., Zhang, L., Wang, J., and Hu, A.: Beijing Climate Center Earth System Model version 1 (BCC-ESM1): model description and evaluation of aerosol simulations, Geoscientific Model Development, 13, 977–1005, https://doi.org/10.5194/gmd-13-977-2020, 2020.

Xing, Y.-F., Xu, Y.-H., Shi, M.-H., and Lian, Y.-X.: The impact of PM2.5 on the human respiratory system, J. Thorac. Dis., 8, E69–74, 2016.

YU, Y.: CAS FGOALS-f3-L model output prepared for CMIP6 CMIP historical, https://doi.org/10.22033/ESGF/CMIP6.3355, 2019.

Yukimoto, S., Kawai, H., Koshiro, T., Oshima, N., Yoshida, K., Urakawa, S., Tsujino, H., Deushi, M., Tanaka, T., Hosaka, M., Yabu, S., Yoshimura, H., Shindo, E., Mizuta, R., Obata, A., Adachi, Y., and Ishii, M.: The Meteorological Research Institute Earth System Model Version 2.0, MRI-ESM2.0: Description and Basic Evaluation of the Physical Component, ournal of the Meteorological Society of Japan. Ser. II, 2019a.

Yukimoto, S., Koshiro, T., Kawai, H., Oshima, N., Yoshida, K., Urakawa, S., Tsujino, H., Deushi, M., Tanaka, T., Hosaka, M., Yoshimura, H., Shindo, E., Mizuta, R., Ishii, M., Obata, A., and Adachi, Y.: MRI MRI-ESM2.0 model output prepared for CMIP6 CMIP historical, https://doi.org/10.22033/ESGF/CMIP6.6842, 2019b.

Zhang, H., Zhang, M., Jin, J., Fei, K., Ji, D., Wu, C., Zhu, J., He, J., Chai, Z., Xie, J., Dong, X., Zhang, D., Bi, X., Cao, H., Chen, H., Chen, K., Chen, X., Gao, X., Hao, H., Jiang, J., Kong, X., Li, S., Li, Y., Lin, P., Lin, Z., Liu, H., Liu, X., Shi, Y., Song, M., Wang, H., Wang, T., Wang, X., Wang, Z., Wei, Y., Wu, B., Xie, Z., Xu, Y., Yu, Y., Yuan, L., Zeng, Q., Zeng, X., Zhao, S., Zhou, G., and Zhu, J.: Description and Climate Simulation Performance of CAS-ESM Version 2, Journal of Advances in Modeling Earth Systems, 12, e2020MS002 210, https://doi.org/https://doi.org/10.1029/2020MS002210, e2020MS002210 2020MS002210, 2020.

Zhang, J., Wu, T., Shi, X., Zhang, F., Li, J., Chu, M., Liu, Q., Yan, J., Ma, Q., and Wei, M.: BCC BCC-ESM1 model output prepared for CMIP6 CMIP historical, https://doi.org/10.22033/ESGF/CMIP6.2949, 2018.

Zhao, A., Ryder, C. L., and Wilcox, L. J.: How well do the CMIP6 models simulate dust aerosols?, Atmospheric Chemistry and Physics, 22, 2095–2119, https://doi.org/10.5194/acp-22-2095-2022, 2022.

Ziehn, T., Chamberlain, M., Lenton, A., Law, R., Bodman, R., Dix, M., Wang, Y., Dobrohotoff, P., Srbinovsky, J., Stevens, L., Vohralik, P., Mackallah, C., Sullivan, A., O'Farrell, S., and Druken, K.: CSIRO ACCESS-ESM1.5 model output prepared for CMIP6 CMIP historical, https://doi.org/10.22033/ESGF/CMIP6.4272, 2019.

Ziehn, T., Chamberlain, M. A., Law, R. M., Lenton, A., Bodman, R. W., Dix, M., Stevens, L., Wang, Y.-P., and Srbinovsky, J.: The Australian Earth System Model: ACCESS-ESM1.5, Journal of Southern Hemisphere Earth Systems Science, 70, 193–214, https://doi.org/10.1071/ES19035, 2020.